Remote Sensing of Environment 135 (2013) 77–91

Contents lists available at SciVerse ScienceDirect

Remote Sensing of Environment

journal homepage: www.elsevier.com/locate/rse

Regional to global assessments of phytoplankton dynamics from the Sea WiFS mission

D.A. Siegel [a,*], M.J. Behrenfeld [b], S. Maritorena [a], C.R. McClain [c], D. Antoine [d], S.W. Bailey [c], P.S. Bontempi [e], E.S. Boss [f], H.M. Dierssen [g], S.C. Doney [h], R.E. Eplee Jr. [c], R.H. Evans [i], G.C. Feldman [c], E. Fields [a], B.A. Franz [c], N.A. Kuring [c], C. Mengelt [j], N.B. Nelson [a], F.S. Patt [c], W.D. Robinson [c], J.L. Sarmiento [k], C.M. Swan [a,1], P.J. Werdell [c], T.K. Westberry [b], J.G. Wilding [c], J.A. Yoder [h]

[a] University of California, Santa Barbara, Santa Barbara, CA 93106-3060, USA
[b] Oregon State University, Corvallis, OR, 97331-2902, USA
[c] NASA Goddard Space Flight Center, Greenbelt, MD 20771, USA
[d] Laboratoire d'Océanographie de Villefranche, 06238 Villefranche sur Mer Cedex, France
[e] NASA Headquarters, Washington, DC 20546, USA
[f] University of Maine, Orono, ME 04469-5706, USA
[g] University of Connecticut, Groton, CT 06340-6048, USA
[h] Woods Hole Oceanographic Institution, Woods Hole, MA 02543, USA
[i] University of Miami, Miami, FL 33149-1098, USA
[j] Ocean Studies Board, The National Academies, Washington, DC 20001, USA
[k] Princeton University, Princeton, NJ 08540-6654, USA

ARTICLE INFO

Article history:
Received 18 January 2012
Received in revised form 13 March 2013
Accepted 25 March 2013
Available online 20 April 2013

Keywords:
Ocean color
SeaWiFS
Phytoplankton
Colored dissolved organic matter
Decadal trends

ABSTRACT

Photosynthetic production of organic matter by microscopic oceanic phytoplankton fuels ocean ecosystems and contributes roughly half of the Earth's net primary production. For 13 years, the Sea-viewing Wide Field-of-view Sensor (SeaWiFS) mission provided the first consistent, synoptic observations of global ocean ecosystems. Changes in the surface chlorophyll concentration, the primary biological property retrieved from SeaWiFS, have traditionally been used as a metric for phytoplankton abundance and its distribution largely reflects patterns in vertical nutrient transport. On regional to global scales, chlorophyll concentrations co-vary with sea surface temperature (SST) because SST changes reflect light and nutrient conditions. However, the ocean may be too complex to be well characterized using a single index such as the chlorophyll concentration. A semi-analytical bio-optical algorithm is used to help interpret regional to global SeaWiFS chlorophyll observations from using three independent, well-validated ocean color data products; the chlorophyll *a* concentration, absorption by CDM and particulate backscattering. First, we show that observed long-term, global-scale trends in standard chlorophyll retrievals are likely compromised by coincident changes in CDM. Second, we partition the chlorophyll signal into a component due to phytoplankton biomass changes and a component caused by physiological adjustments in intracellular chlorophyll concentrations to changes in mixed layer light levels. We show that biomass changes dominate chlorophyll signals for the high latitude seas and where persistent vertical upwelling is known to occur, while physiological processes dominate chlorophyll variability over much of the tropical and subtropical oceans. The SeaWiFS data set demonstrates complexity in the interpretation of changes in regional to global phytoplankton distributions and illustrates limitations for the assessment of phytoplankton dynamics using chlorophyll retrievals alone.

1. Introduction

The open ocean accounts for nearly 70% of the Earth's surface and phytoplankton dominate the autotrophic production of the marine ecosystems, accounting for roughly half of the Earth's annual net primary production (e.g., Behrenfeld et al., 2001; Field et al., 1998). This conversion of CO_2 into organic matter fuels the metabolic demands of marine ecosystems and drives ocean biogeochemical cycles. Global phytoplankton production depends on the availability of sunlight and nutrients (e.g., nitrogen, phosphorous, iron), and thus is sensitive to changes in the physical processes regulating these resources (e.g., Behrenfeld et al., 2001, 2006; Boyce et al., 2010; Martinez et al., 2009; Vantrepotte & Mélin, 2009; Yoder & Kennelly, 2003).

The response of phytoplankton to environmental changes can be rapid. Under light- and nutrient-replete growth conditions, phytoplankton abundances can double within a single day, leading to intense blooms. These rapid increases in phytoplankton standing

* Corresponding author. Tel.: +1 805 893 4547.
E-mail address: davey@eri.ucsb.edu (D.A. Siegel).
[1] Present address: Institute of Biogeochemistry and Pollutant Dynamics, ETH Zürich, Switzerland.

0034-4257
http://dx.doi.org/10.1016/j.rse.2013.03.025

stocks are often followed by rapid declines, as resources are exhausted and grazers and other export processes consume phytoplankton. This balance between phytoplankton growth and loss processes controls the magnitude of the response of phytoplankton populations to environmental changes on seasonal to decadal time scales (e.g., Behrenfeld, 2010; Behrenfeld et al., 2006, 2008; Falkowski et al., 1998; Martinez et al., 2009; Polovina et al., 2008; Siegel et al., 2002a).

Observing changes in global phytoplankton distributions is challenging at best. Research vessels travel at roughly the speed of a bicycle, have limited geographic range, and are costly to operate, making them impractical for long-term, sustained, global surveying. Autonomous sampling platforms equipped with sensors capable of measuring relevant ocean ecosystem parameters have been developed (e.g., Bishop et al., 2002; Johnson et al., 2009) but these advances are relatively recent and appropriate data over the global ocean are not yet available. Global observations of phytoplankton dynamics have resulted largely from satellite ocean color sensors that sample the entire Earth surface in just a few days (McClain, 2009).

The longest and most complete satellite ocean color record stems from the Sea viewing Wide-Field of view Sensor (SeaWiFS), which was launched on August 1, 1997 and operated until December 14, 2010. A key objective for the SeaWiFS mission was the determination of surface layer phytoplankton chlorophyll *a* concentration (hereafter referred to simply as chlorophyll). The standard SeaWiFS chlorophyll product is based on an empirical band-ratio algorithm (O'Reilly et al., 1998). The basic principle of the algorithm is that ocean remote sensing reflectance at blue wavelengths decreases relative to the green wavelengths, as phytoplankton concentrations increase, due to absorption by chlorophyll and other constituents. The ratio between these two bands is used to quantify the chlorophyll concentration.

An underlying assumption in the band ratio approach is that changes in ocean color can be described using a single index — the chlorophyll concentration (Morel, 1988; Smith & Baker, 1978). This presumes that all optically active materials covary with the chlorophyll concentration, which may not hold under all situations or for future oceans (Dierssen, 2010; Lee et al., 2002, 2010; Morel et al., 2010; Sauer et al., 2012; Siegel et al., 2002b, 2005a; Szeto et al., 2011). Non-living materials, such as Colored Dissolved Organic Matter (CDOM) and nonviable, detrital particulate materials, dominate ocean color signals for some wavelengths and these materials can vary independently from changes in chlorophyll concentration (Bricaud et al., 2011; Morel et al., 2010; Nelson & Siegel, 2013; Siegel et al., 2005a, 2005b). An example of the contributions made by different optical components to the mean total absorption spectrum is shown in Fig. 1 where the component absorption spectrum observations are from a consistent, open ocean, in situ data set that spans the upper layers (≤30 m) from all of the major ocean basins (N = 371; data from Nelson et al., 1998, 2007, 2010; Swan et al., 2009; Nelson & Siegel, 2013). The gray envelopes in Fig. 1 represent the 95% confidence interval for each mean estimate. For wavelengths less than 490 nm, CDOM is by far the most important factor contributing to total absorption in the open ocean and, on the average, 60% of the total light absorption at 400 nm is due to CDOM (Fig. 1). Phytoplankton absorption never dominates the mean spectral light absorption budget and only for wavelengths greater than 490 nm does its contribution approach that of CDOM. Throughout the visible spectrum, the contribution of CDOM is also much greater than the absorption by inanimate, detrital particulates, which make a much smaller contribution throughout the visible spectrum (detrital absorption is <10% of the total absorption coefficient). Thus, nonliving optical signals are an important consideration in the assessment of phytoplankton dynamics from global ocean color observations.

Phytoplankton optical properties are also functions of their size, shape, cellular pigment composition and concentration, which are in turn regulated by the assemblage of phytoplankton species present and their physiological state (e.g., Behrenfeld et al., 2005, 2008; Bricaud et al., 2004; Ciotti et al., 2002; Dierssen, 2010; Falkowski, 1984; Kirk, 1994; Morel & Bricaud, 1981; Stramski et al., 2004). In particular, phytoplankton can adjust their intracellular chlorophyll content in response to light and nutrients (e.g., Behrenfeld et al., 2005; Laws & Bannister, 1980). When growth irradiance decreases and nutrients remain replete, phytoplankton increase their chlorophyll content to more efficiently capture light. When nutrients become scarce, they reduce their chlorophyll in direct proportion to their nutrient-defined growth rate (e.g., Halsey et al., 2010; Laws & Bannister, 1980). Together these physiological adjustments can introduce more than a ten-fold variation in phytoplankton chlorophyll to carbon ratios, which will hinder our ability to interpret changes in phytoplankton biomass from observations of chlorophyll concentrations.

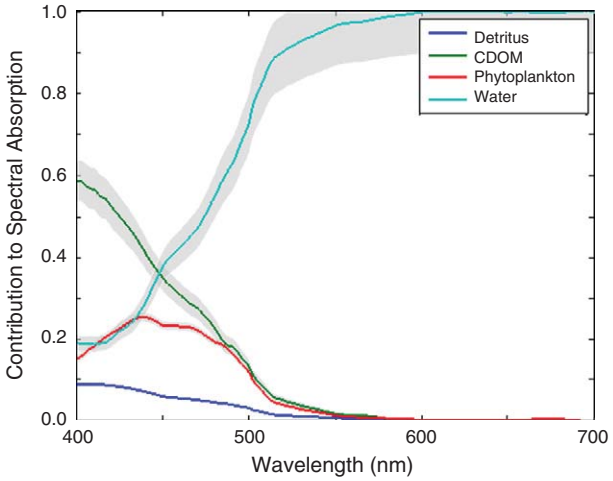

Fig. 1. Global mean fractional contributions made by phytoplankton ($a_{ph}(\lambda)$; red), colored dissolved organic matter (CDOM; $a_g(\lambda)$; blue), detrital particulates ($a_{det}(\lambda)$; blue), and seawater ($a_w(\lambda)$; light blue) to the total absorption ($a_{tot}(\lambda) = a_{det}(\lambda) + a_{ph}(\lambda) + a_g(\lambda) + a_w(\lambda)$) at that same wavelength. The gray envelopes are 95% confidence intervals for the mean spectra. A total of 371 coincident observations of $a_{det}(\lambda)$, $a_{ph}(\lambda)$ and $a_g(\lambda)$ from the upper 30 m are used to develop the global, open ocean composite of fractional contributions to spectral light absorption. Absorption spectra are compiled from the Atlantic, Pacific, Indian and Southern Oceans (CLIVAR cruises A20, A22, P16N, P16S, P18 and I8S, the African Monsoon Multidisciplinary Analyses (AMMA) cruise to the equatorial Atlantic and the Bermuda Atlantic Time Series Study (BATS)). Methods and further details are presented in Nelson et al. (1998), Nelson et al. (2007), Nelson et al. (2010), Swan et al. (2009) and Nelson and Siegel (2013).

Here we present a synthesis of SeaWiFS observations focused on documenting and interpreting regional- to global-scale change in ocean phytoplankton distributions. We summarize how the SeaWiFS mission achieved a climate-quality record of ocean remote sensing reflectance spectra (referred to as 'ocean color') and how ocean color observations are used to retrieve phytoplankton chlorophyll concentrations. We discuss changes in the ocean biosphere indicated by the standard SeaWiFS chlorophyll algorithm product and show that spurious interpretations may result from not assessing other important bio-optical signals. Our analyses highlight the spatial heterogeneity of phytoplankton responses to ocean climate variations, demonstrate the importance of non-phytoplankton absorption in ocean color signals and illustrate the relative importance of physiology and biomass changes on observed chlorophyll concentrations and the interpretation of phytoplankton dynamics from ocean color observations. We conclude with a discussion of steps to ensure continued observation and future paths for new discoveries of the ocean biosphere.

2. Data and methods

2.1. SeaWiFS observations of remote sensing reflectance

SeaWiFS was a polar-orbiting, sun-synchronous, crosstrack-scanning instrument with six visible "ocean color" wavebands and two near-

infrared (NIR) "atmospheric correction" bands (McClain et al., 2004). SeaWiFS collected imagery at a nominal 1-km spatial resolution (globally subsampled to 4 km) and achieved near-complete global measurement coverage every 2 days. Accurate ocean color retrievals are among the most difficult Earth-system satellite data to acquire, in part because only ~10% of the signal measured by the satellite sensor at the top-of-atmosphere originates from the ocean (the remaining ~90% comes from the atmosphere and surface reflectance). SeaWiFS's NIR bands provide critical data for removing the atmospheric contribution to radiances measured at the 6 ocean color bands. Sensor calibration and characterization (pre- and post-launch) and corrections to remove the effects of scattering and absorption by the atmosphere and reflection from the ocean surface have proven crucial for creating high quality determinations of the spectral reflectance emanating from the ocean.

The SeaWiFS mission pioneered two system calibration procedures that helped it achieve the accuracy and stability required for climate science (McClain, 2009; McClain et al., 2004; National Research Council, 2011). First, relative changes of the SeaWiFS's calibration were monitored by monthly viewing of the moon at constant phase and each spectral band was characterized to ~0.1% over the mission's lifetime (Eplee et al., 2011). Second, absolute system calibration factors were determined through a vicarious calibration (Franz et al., 2007), which compares satellite observations to high-quality field measurements of ocean remote sensing reflectance propagated to the top of the atmosphere. Following this approach, uncertainties in absolute calibration factors are within 0.3% for all visible bands and resultant retrievals of ocean remote sensing reflectance have uncertainties of ~3% for conditions similar to the field calibration site (see Supplementary Information section).

2.2. The SeaWiFS chlorophyll algorithm (OC4v6)

The 'standard' SeaWiFS chlorophyll product, Chl_{OC4}, is based on an empirical, maximal band-ratio algorithm (O'Reilly et al., 1998) using remote sensing reflectance measurements at 443, 490, 510 and 555 nm. This algorithm, OC4v6, empirically relates the maximum of three remote sensing reflectance band-ratios, 443/555, 490/555 and 510/555, to the chlorophyll concentration (see http://oceancolor.gsfc.nasa.gov/REPROCESSING/R2009/ocv6/). For low chlorophyll waters, the 443/555 ratio will be the maximum ratio used, whereas for eutrophic waters the 510/555 ratios will be selected. The maximum band-ratio approach proved to be very effective for accurately retrieving chlorophyll concentrations over a very large dynamic range (e.g., O'Reilly et al., 1998). Nearly 2000 paired observations of ocean remote sensing reflectance and chlorophyll concentration from version 2 of the NASA bio-Optical Marine Data set (NOMADv2) archive of bio-optical field measurements (Werdell & Bailey, 2005) were used to derive the OC4v6 algorithm.

Performance of the OC4v6 algorithm is excellent (Table 1) when applied to the NOMADv2 data set of ocean remote sensing reflectance spectra and compared with the in situ chlorophyll measurements (http://seabass.gsfc.nasa.gov/seabasscgi/nomad.cgi). This in situ data comparison can be thought of as measuring the inherent variability in the OC4v6 algorithm, as the NOMADv2 observations comprised nearly all of the data used to determine the OC4v6 model coefficients.

SeaWiFS remote sensing reflectance spectra can be also used to assess the performance of the OC4v6 algorithm. A matchup data set of SeaWiFS remote sensing reflectance spectra and in situ observations (largely from NOMADv2) is constructed using the single level-3 pixel (~9 km) containing the in situ observation for that day. The performance of the Chl_{OC4} algorithm is again excellent (Table 1); with an R^2 value of 0.795, slopes approaching unity, and a log-transformed intercept near zero. Similar validation results for Chl_{OC4} are found in the analyses conducted by the NASA Ocean Biology Processing Group following procedures laid out by Bailey & Werdell, 2006. Thus, the SeaWiFS band ratio chlorophyll algorithm (OC4v6) has excellent performance when compared with the NOMADv2 in situ chlorophyll data, both using in situ reflectance determinations and SeaWiFS reflectances.

Table 1
Validation for bio-optical models using in situ and SeaWiFS satellite remote sensing reflectance observations.

Parameter	N	Intercept	Slope	R^2	RMS deviation	Bias
Validation using in situ remote sensing reflectance observations						
Chl_{OC4}	2687	−0.008	0.975	0.859	0.275	−0.005
Chl_{GSM}	2528	−0.058	1.040	0.850	0.292	−0.063
CDM	878	0.097	1.115	0.850	0.256	−0.032
BBP	314	0.424	1.160	0.632	0.197	0.014
Validation using SeaWiFS remote sensing reflectance observations						
Chl_{OC4}	1543	−0.011	0.981	0.795	0.310	−0.008
Chl_{GSM}	1380	−0.175	0.958	0.774	0.363	−0.165
CDM	484	0.239	1.170	0.566	0.336	0.014
BBP	201	0.047	1.048	0.531	0.210	−0.071

All comparisons are made comparing $\log_{10}$-transformed variables. In situ validation is done using ocean remote sensing reflectance determinations from an updated version of the NOMAD data set (NOMADv2; following Werdell & Bailey, 2005) Matchups with satellite remote sensing reflectance values are calculated using the single level-3 (9 km) pixel containing the observation for that day and the NOMADv2 field observations.

2.3. The Garver–Siegel–Maritorena ocean color algorithm and its interpretation

Advances in ocean optics modeling have yielded tools to decompose satellite ocean color signals into multiple, specific optical contributions (e.g., IOCCG, 2006). Here, the Garver–Siegel–Maritorena algorithm (GSM; Maritorena et al., 2002, 2010) is applied to SeaWiFS ocean reflectance data to estimate chlorophyll concentration (Chl_{GSM}), the combined absorption at 443 nm by CDOM and detrital particulates (CDM), and the particulate backscattering coefficient at 443 nm (BBP). The GSM model retrieves Chl_{GSM}, CDM and BBP simultaneously by performing a non-linear least-squares minimization between the satellite and modeled reflectance for all available visible bands. Model parameters were evaluated through a constrained optimization using observed remote sensing reflectance, chlorophyll, CDM and BBP determinations mostly from open ocean, non-polar environments (Maritorena et al., 2002). Our goal in applying the GSM model is to elucidate phytoplankton chlorophyll changes independently from CDM (Siegel et al., 2005a), while providing a proxy for phytoplankton carbon biomass using BBP (Behrenfeld et al., 2005).

The performance of the GSM algorithm can be evaluated using both in situ and satellite data. Using the NOMADv2 in situ reflectance spectra, the GSM retrievals of chlorophyll concentrations are excellent, with performance metrics that are nearly equivalent to those of the operational SeaWiFS algorithm (Table 1). This is a noteworthy accomplishment considering that the GSM parameters are optimized to simultaneously retrieve values of Chl_{GSM}, BBP and CDM, not just chlorophyll concentration (Maritorena et al., 2002). Further, very few of the observations used by Maritorena et al. (2002) to optimize the GSM model are contained in the NOMADv2 data set (44 of 1024). The GSM algorithm also performs very well in terms of CDM retrievals based on the NOMADv2 data set, while uncertainties are somewhat greater for the BBP product (although there are also far fewer field BBP data available; Table 1).

End-to-end performance of the Chl_{GSM} retrievals for SeaWiFS ($R^2 = 0.774$) is nearly as good as the OC4v6 retrievals although a small bias is observed (Table 1). However, GSM model performance with the satellite matchup data for the two other data products is not as good as found using in situ data. Differences in performance between the OC4v6 and the GSM model are expected because the GSM model works on absolute reflectance values, while OC4v6 algorithm uses ratios of reflectance determinations. Hence, GSM retrievals will be more sensitive to noise in the reflectance retrievals than

band-ratio based algorithms. Satellite spectral reflectance data are generally noisier than in situ measurements, particularly in areas where atmospheric correction is problematic (e.g., Gordon, 1997) or in the open ocean where the selection of digitization levels of the NIR bands for SeaWiFS creates noise in open ocean chlorophyll retrievals (Hu et al., 2001). These issues clearly affect the quality of GSM retrievals. Overall the GSM model applied to the SeaWiFS reflectance observations performs well when compared with the NOMADv2 matchup data set, particularly for Chl_{GSM} (Table 1).

Retrievals of colored dissolved and detrital organic material (CDM) are dominated by the dissolved fraction (CDOM) in open ocean waters (Fig. 1; Siegel et al., 2002b; Nelson et al., 2010; Nelson & Siegel, 2013). The mean value for the ratio of the detrital particulate absorption coefficient at 443 nm to CDM from the global, open ocean, in situ data shown in Fig. 1 is 16.5% (std. dev. = 13.1%; N = 371). Hence variations in retrieved CDM values will be dominated by changes in the CDOM concentration.

The particulate backscattering coefficient (BBP) is used as a proxy for changes in phytoplankton carbon biomass as there are very few direct measurements of phytoplankton carbon concentrations that can be used to derive empirical algorithms (e.g., Behrenfeld et al., 2005; Westberry et al., 2008). Several observations support the application of the BBP proxy for phytoplankton carbon biomass. First, a related optical property, the particulate beam attenuation coefficient at 660 nm (c_p) is most sensitive to particles in the size range ~0.5–20 μm (Stramski & Kiefer, 1991), a window which overlaps most phytoplankton found in the open ocean. Changes in c_p have repeatedly been shown to track phytoplankton growth and abundance over diel cycles (Durand & Olson, 1996; Gernez et al., 2011; Green et al., 2003; Siegel et al., 1989) and values of the chlorophyll normalized c_p (c_p:Chl) are strongly correlated with phytoplankton photosynthetic indices (Behrenfeld & Boss, 2003, 2006). Thus, there is a strong body of evidence linking changes in c_p and phytoplankton biomass. More recently, regional observations have shown relationships between c_p and BBP (Antoine et al., 2011; Dall'Olmo et al., 2009, 2011; Westberry et al., 2010). Thus, changes in BBP in the open ocean should be strongly linked to changes in phytoplankton biomass (see also Behrenfeld et al., 2005; Westberry et al., 2008; Huot et al., 2008). Such relationships will not necessarily apply in coastal regions where there is substantial inputs of terrigenous material or for regions of the world ocean where particulate backscattering is influenced by coccolithophore abundances (e.g., Balch et al., 2011). However for much of the world ocean, BBP will be a useful proxy for phytoplankton biomass.

2.4. Specific data and analyses employed

Monthly level-3 imagery (~9 km) from the SeaWiFS mission is used for this analysis (version 2010.0; http://oceancolor.gsfc.nasa.gov). Monthly images are used from October 1997 to November 2010, although after January 2008 there are several months of missing observations due to various spacecraft and communication issues. Data products include ocean remote sensing reflectance at 412, 443, 490, 510, 555 and 670 nm, the operational chlorophyll concentration (Chl_{OC4}), and the daily incident flux of photosynthetically available radiation (PAR). Sea surface temperature (SST) fields were available from the Advanced Very High Resolution Radiometer (AVHRR) Pathfinder version 5.2 at a 4 km spatial resolution. Only nighttime SST imagery is used to minimize effects of diurnal heating.

All ocean color satellite data were also mapped and averaged into 1° by 1° latitude/longitude bins prior to analysis defining the regional bins used in this analysis. All algorithms were applied to the level-3 binned ocean remote sensing reflectance spectra before mapping and averaging into 1° regional bins. Values of Chl_{OC4}, Chl_{GSM}, and CDM were log-transformed before averaging following Campbell (1995). Estimates of median mixed layer growth irradiance, I_g, are determined as PAR $\exp(-K_{PAR}\,MLD/2)$, where K_{PAR} follows Morel et al. (2007) and MLD determinations are from the Fleet Numerical Oceanography Center model output (Clancy & Sadler, 1992). Monthly anomalies were calculated as the difference between monthly mean values for each regional bin and the mission-long monthly mean for that bin. Global aggregate anomalies for the warm/cool oceans, based upon the locations of the mission mean 15 °C SST isotherm, were calculated from the regional binned anomalies after accounting for differences in the latitudes of the regional bins (Behrenfeld et al., 2006). All trend calculations were made by type 1 linear regression and only significant (by the 95% c.i.) trends are shown. Trends in log-transformed variables are presented in % per year, noting that the change in a natural log transformed variable is equivalent to the normalized rate of change (Campbell, 1995).

3. Results

3.1. Observations using the SeaWiFS operational chlorophyll products

The mean band ratio chlorophyll concentration (Chl_{OC4}) for the SeaWiFS mission illustrates several important features of the global ocean biosphere (Fig. 2). First, the spatial distribution of chlorophyll largely reflects broad-scale patterns in wind-driven vertical transports of nutrients (e.g., McClain, 2009; Sverdrup, 1955; Yoder et al., 1993). Prominent regions of low chlorophyll are found in the subtropical gyres, where downwelling Ekman pumping prevails. In contrast, regions of deep seasonal mixing (e.g., high latitudes) or persistent upwelling (e.g., along equator, Arabian Sea, eastern boundary currents) exhibit elevated chlorophyll levels (Fig. 2). Second, spatial differences in mean Chl_{OC4} values span nearly 2 orders of magnitude — from 0.03 to >1 mg m^{-3} with a near log-normal distribution. Third, the 15 °C SST mean isotherm (black line in Fig. 2) effectively delineates the productive, high-chlorophyll sub-polar and polar regions from the nutrient-impoverished, low-chlorophyll regions of the tropics and subtropics (as in Behrenfeld et al., 2006).

SeaWiFS was launched during the peak of a strong El Niño and the relaxation to the cooler, La Niña phase was the primary driver for observed global increases in surface chlorophyll during the early years of the mission (e.g., Behrenfeld et al., 2001; Yoder & Kennelly, 2003). Following the La Niña, mean ocean temperatures oscillated between minor warming and cooling periods, while chlorophyll levels tracked fluctuations in SST (e.g., Behrenfeld et al., 2006; Gregg et al., 2005; Martinez et al., 2009). Relationships between SST and Chl_{OC4} are easily seen in the monthly anomalies for the three global aggregates: the cool northern hemisphere (NH) region (mean SST < 15 °C; Fig. 3a), the warm, permanently-stratified ocean (mean SST > 15 °C; Fig. 3b), and the cool southern hemisphere (SH) (mean SST < 15 °C; Fig. 3c). Note that the SST axis for each panel in Fig. 3 is inverted to illustrate the correspondence between Chl_{OC4} and -SST monthly anomalies. All three global aggregates exhibit strong interannual patterns, with the 1998–99 El Niño–La Niña transition from warm to cool SST values (and from low to high Chl_{OC4} retrievals) being most clearly seen in the warm ocean aggregate. In fact for all three global aggregate regions, monthly anomalies for Chl_{OC4} are significantly correlated with changes in SST, where an inverse relationship is found for the warm and cool NH oceans but a positive relationship is found for the cool SH ocean (Table 2). Note that SST is considered here as a proxy for changes in physical ocean conditions, where anomalously warm SST's are associated with decreasing mixed layer depth, suppressed surface nutrient input, and higher average light exposure for the near-surface mixed layer.

Highly significant, increasing linear trends in SST are found for all three global aggregates, varying from 0.015 to 0.035 °C per year and with the greatest increases occurring in the cool NH ocean (Fig. 3; Table 3). At the same time, statistically significant decreasing trends in Chl_{OC4} are found only over the warm ocean aggregate ($-0.18\%\ year^{-1}$) while

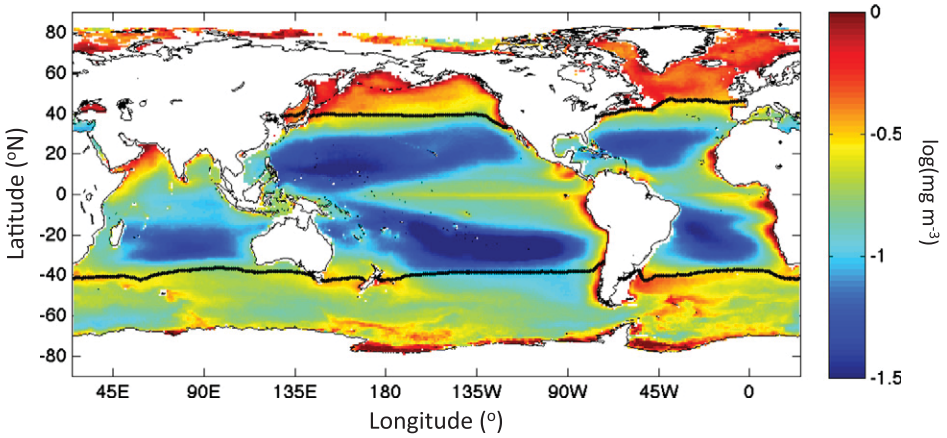

Fig. 2. Mission mean chlorophyll concentration from SeaWiFS from August 1, 1997 to December 14, 2010. The OC4v6 band-ratio Chl algorithm (Chl_{OC4}) is used. Mean values of $\log(Chl_{OC4})$ are calculated for 1° bins in latitude and longitude over the global ocean. Units are $\log_{10}(mg\ m^{-3})$. The location of the mean SST = 15 °C isotherm is shown as the black lines. This is an update of figure 3.36a from Siegel et al. (2011) using the 2010.0 version of the SeaWiFS data set.

increasing trends are observed in the cool SH (trend = 0.83% $year^{-1}$) and insignificant trends for the cool NH aggregate (Table 3).

The global aggregates (Fig. 3) provide an integrated view of net relationships between ocean biology and physical ocean conditions, but they do not illustrate these processes on regional scales (here defined as 1° bins in latitude and longitude). The correlation between Chl_{OC4} and SST regional scale anomalies shows extensive regions of both negative and positive correlations (Fig. 4a). The dominant pattern in the warm stratified ocean is an inverse correlation between Chl_{OC4} and SST anomalies (blue in Fig. 4a), with only small regions of positive correlation (red regions in Fig. 4a; e.g., west of Central America, between Madagascar and Western Australia). In contrast, the cool NH and SH waters show coherent regions of both positive and negative correlations, although much of the two cool global ocean aggregates show no significant correlation. Again, the 15 °C SST isotherm (black lines in Fig. 4a) approximately delineates the warm ocean where predominantly inverse correlations are found from the rest of the oceans.

Regional temporal trends of $\log(Chl_{OC4})$ over the 13 years of the SeaWiFS record show large areas of both increasing (red areas in Fig. 4b) and decreasing (blue areas) values. These regional trend patterns show some resemblance with the spatial distribution of SST trends (Fig. 4c) and are consistent with those analyzed by Vantrepotte & Mélin, 2009 using the first 10 years of the SeaWiFS data record (their Fig. 6b). The two trend estimates show a weak significant, inverse correlation from the warm ocean aggregate ($R^2 = 0.077$, $p < 0.001$), but this relationship explains a very small amount of variability. For the two cool ocean basins, correspondence between the regional scale trends is even more tenuous. Clearly, the aggregate trends of Fig. 3 have many underlying regional nuances, with magnitudes ten-fold greater than the global summaries. These regional areas of large decadal trends in Chl_{OC4} (absolute values > 30% over a decade; Fig. 4b) are likely caused by migration of boundaries between bio-optical provinces in response to regional changes in physical ocean climate. Clearly, the spatial variability in regional scale trends in Chl_{OC4} (Fig. 4b) demonstrates the challenges in assessing global ocean biosphere changes from a sparse array of observational assets.

3.2. CDM and the remote sensing of chlorophyll

The SeaWiFS operational chlorophyll products provide a first-order view of phytoplankton dynamics on regional to global scales. However, the SeaWiFS algorithm assumes a fixed relationship among optical properties, which may not hold in all conditions (e.g., Dierssen, 2010; Siegel et al., 2002b, 2005b; Szeto et al., 2011). To evaluate the importance of independence among optical properties, we use the GSM ocean color algorithm, which enables phytoplankton chlorophyll changes to be quantified separately from absorption due to CDOM and detrital particles, while providing an independent measure of phytoplankton carbon biomass via the particulate backscattering coefficient. The GSM data products are presented here to provide greater insights into the processes regulating phytoplankton dynamics.

The significance of variable CDM absorption on global chlorophyll retrievals can be illustrated using the normalized difference between the band ratio and the GSM-derived chlorophyll concentrations, ΔChl_{norm} (Fig. 5a; after Siegel et al., 2005b). The mean ΔChl_{norm} distribution shows that Chl_{OC4} retrievals are ~20% lower than Chl_{GSM} within the subtropical gyres, while Chl_{OC4} retrievals are considerably higher than Chl_{GSM} values in the subpolar oceans, with differences of more than 60% occurring in the northern hemisphere. Again, the 15 °C SST isotherm effectively delineates these two regions (black lines in Fig. 5a).

Many of the differences between the chlorophyll retrievals can be explained by the presence of CDM as retrieved by the GSM model. The mean distribution of the fraction of non-water light absorption at 443 nm regulated by CDM (%CDM) varies from ~40 to more than 70% (Fig. 5b). As demonstrated previously, values of %CDM are low in the subtropical gyres and higher at higher latitudes (Siegel et al., 2002b, 2005b). Importantly, the mean spatial distribution of ΔChl_{norm} looks very similar to the mean %CDM distribution, with their correspondence being particularly dramatic at high northern latitudes and the correlation between the two mean spatial patterns is highly significant ($R = +0.738$; $p < 0.001$). On a regional scale, temporal changes in ΔChl_{norm} are also highly correlated with changes in %CDM, revealing a strong positive correlation throughout the warm ocean (where mean SST > 15 °C; Fig. 5c). Correlations between regional changes in %CDM and ΔChl_{norm} are not as strong in either of the cool ocean domains. Together, these data confirm the need to account for CDM influences on assessments of phytoplankton dynamics from satellite ocean color observations (e.g., Sauer et al., 2012; Siegel et al., 2005b; Szeto et al., 2011).

3.3. Global to regional scale variability of CDM-partitioned chlorophyll

The GSM model provides chlorophyll determinations independent from the competing influences of CDM. The correspondence between interannual trends in monthly anomalies in Chl_{GSM} and CDM and sea surface temperature (SST) are shown for the cool NH aggregate (Fig. 6a, b), the warm, permanently-stratified ocean (Fig. 6c, d), and the cool SH ocean (Fig. 6e, f). As before, all three global aggregates exhibit strong interannual patterns, with the 1998–99 El Niño–La Niña transition from warm to cool SST values (and from low to high Chl_{GSM} retrievals) being most clearly seen in the warm ocean aggregate.

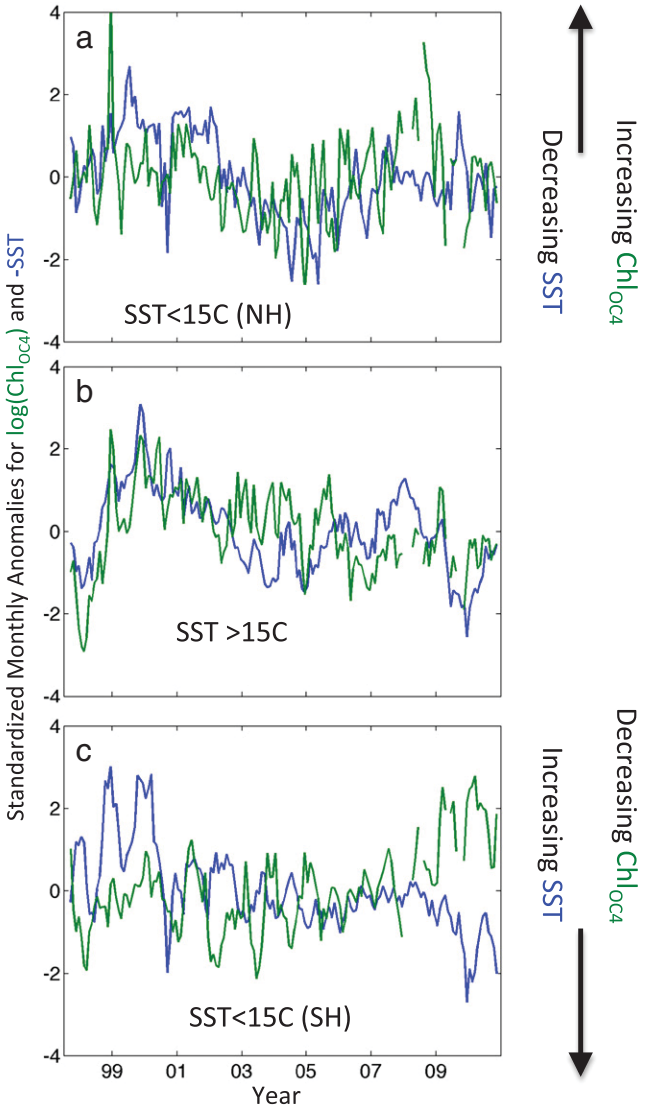

Fig. 3. Time series of Chl_{OC4} and sea surface temperature (SST) monthly standardized anomalies (z-scores) for three global regions delineated by the mean SST isotherm for a) the cool (mean SST < 15 °C) northern hemisphere (NH) aggregate, b) the warm, permanently-stratified ocean aggregate (mean SST > 15 °C) and c) the cool southern hemisphere (SH) (mean SST < 15 °C). Anomalies are constructed by first removing the monthly mean value for each 1 degree bin of each property and then aggregating the regional, monthly anomalies into global aggregates. Statistics of the correlations between log(Chl_{OC4}) and SST monthly anomalies are given in Table 2 and mission length trend analyses are presented in Table 3. This is an update of figure 3.37 from Siegel et al. (2011) using the 2010.0 version of the SeaWiFS data set and the AVHRR Pathfinder v5.2 data set.

Further, changes in both Chl_{GSM} and CDM show correspondence with changes in SST for the other two global aggregates (Fig. 6).

The covariation of both Chl_{GSM} and CDM with SST is not unexpected (e.g., Behrenfeld et al., 2005, 2008; Nelson & Siegel, 2013; Siegel et al., 2005a; Swan et al., 2009). As the physical ocean decreases mixed layer depth and inhibits vertical mixing (leading to elevated SST), subsurface nutrient fluxes are suppressed and average light levels for the near-surface mixed layer increases. These factors will reduce retrievals of both Chl_{GSM} and CDM through the processes of phytoplankton physiological acclimation and photobleaching of CDOM, respectively (e.g., Nelson & Siegel, 2013; Siegel et al., 2005a). When the mixed layer depth increases and vertical mixing intensifies (leading to reductions in SST), new nutrients and CDOM are transported into the euphotic zone leading to strong increases of both Chl_{GSM} and CDM.

The correlations found between interannual anomalies in CDM and SST for the permanently stratified oceans ($R = -0.762$; $p < 0.001$; Fig. 6d) are the strongest found in this study (Table 2). Strong negative correlations are also found between CDM and SST for the cool NH region ($R = -0.297$; $p < 0.001$; Fig. 6b). In both cases, warming is associated with decreasing CDM and cooling with increasing CDM. This is consistent with greater photobleaching of CDOM in shallower mixed layers due to enhanced average light levels (e.g., Nelson & Siegel, 2013; Siegel et al., 2002b, 2005a; Swan et al., 2009, 2012). The strongest relationships between SST and Chl_{GSM} anomalies are found for the permanently stratified oceans ($R = -0.543$; $p < 0.001$; Fig. 6c) and the cool SH region ($R = +0.377$; $p < 0.001$; Fig. 6e). In the warm ocean aggregate, Chl_{GSM} and SST changes are again inversely related, which is consistent with physiological responses of phytoplankton to increasing light and decreasing nutrients (Behrenfeld et al., 2008). In the cool SH, chlorophyll anomalies are positively correlated with SST changes, indicating that a warming surface layer is associated with improved conditions for biomass accumulation (either reflecting increased availability of a limiting resource for growth or ecosystem-level changes in phytoplankton growth-loss relationships; Doney, 2006; Behrenfeld, 2010).

As shown previously, highly significant, increasing SST trends are observed for all three global aggregates over the SeaWiFS era (Table 3). Statistically significant increases in Chl_{GSM} are observed in the cool NH (trend = 0.80% $year^{-1}$; Fig. 6a) and the cool SH oceans (trend = 1.10% $year^{-1}$; Fig. 6e), while long-term trends for Chl_{GSM} over the warm ocean aggregate were statistically insignificant (Fig. 6c; Table 3). Conversely, CDM trends over the SeaWiFS era decreased within both the warm ocean (−0.31% $year^{-1}$; Fig. 6d) and the cool NH ocean region (−0.56% $year^{-1}$; Fig. 6f), while the trends in CDM over time were insignificant for the cool SH aggregate (Table 3).

Again, regional-scale correlations between Chl_{GSM} and SST anomalies show large regions of both negative and positive correlations (Fig. 7a) and look very similar (although slightly muted) to linear correlation

Table 2
Correlations coefficients (R) between time series of monthly anomalies of SST and SeaWiFS retrievals for the three global aggregates.

	Chl_{OC4}		Chl_{GSM}		CDM	
Region	R	p-Value	R	p-Value	R	p-Value
SST < 15 °C NH	**−0.2496**	0.0019	+0.0566	0.4879	**−0.2967**	0.0002
SST > 15 °C	**−0.5539**	<0.0001	**−0.5427**	<0.0001	**−0.7620**	<0.0001
SST < 15 °C SH	**+0.3013**	0.0002	**+0.3772**	<0.0001	+0.0480	0.5599

Correlation values are bolded for p values less than 0.05.

Table 3
Trends in the three SeaWiFS retrievals and SST vs. time over the SeaWiFS mission.

Region	Slope	95% confidence interval for Slope		R^2	p-Value
SST (slope units = °C/year)					
SST < 15 °C NH	**0.0352**	0.0229	0.0476	**0.1684**	<0.0001
SST > 15 °C	**0.0152**	0.0101	0.0202	**0.1824**	<0.0001
SST < 15 °C SH	**0.0288**	0.0234	0.0341	**0.4165**	<0.0001
Chl_{OC4} (slope units = %/year)					
SST < 15 °C NH	0.0373	−0.2702	0.3449	0.0004	0.8107
SST > 15 °C	**−0.1758**	−0.3061	−0.0455	**0.0453**	0.0085
SST < 15 °C SH	**0.8300**	0.6217	1.0383	**0.2924**	<0.0001
Chl_{GSM} (slope units = %/year)					
SST < 15 °C NH	**0.7960**	0.4605	1.1314	**0.1278**	<0.0001
SST > 15 °C	−0.0803	−0.1696	0.0089	0.0206	0.0774
SST < 15 °C SH	**1.0981**	0.8771	1.3192	**0.3911**	<0.0001
CDM (slope units = %/year)					
SST < 15 °C NH	**−0.5587**	−0.8689	−0.2484	**0.0778**	0.0005
SST > 15 °C	**−0.3136**	−0.4190	−0.2082	**0.1871**	<0.0001
SST < 15 °C SH	−0.0428	−0.1800	0.0945	0.0025	0.5391

Correlation values are bolded for p values less than 0.01.

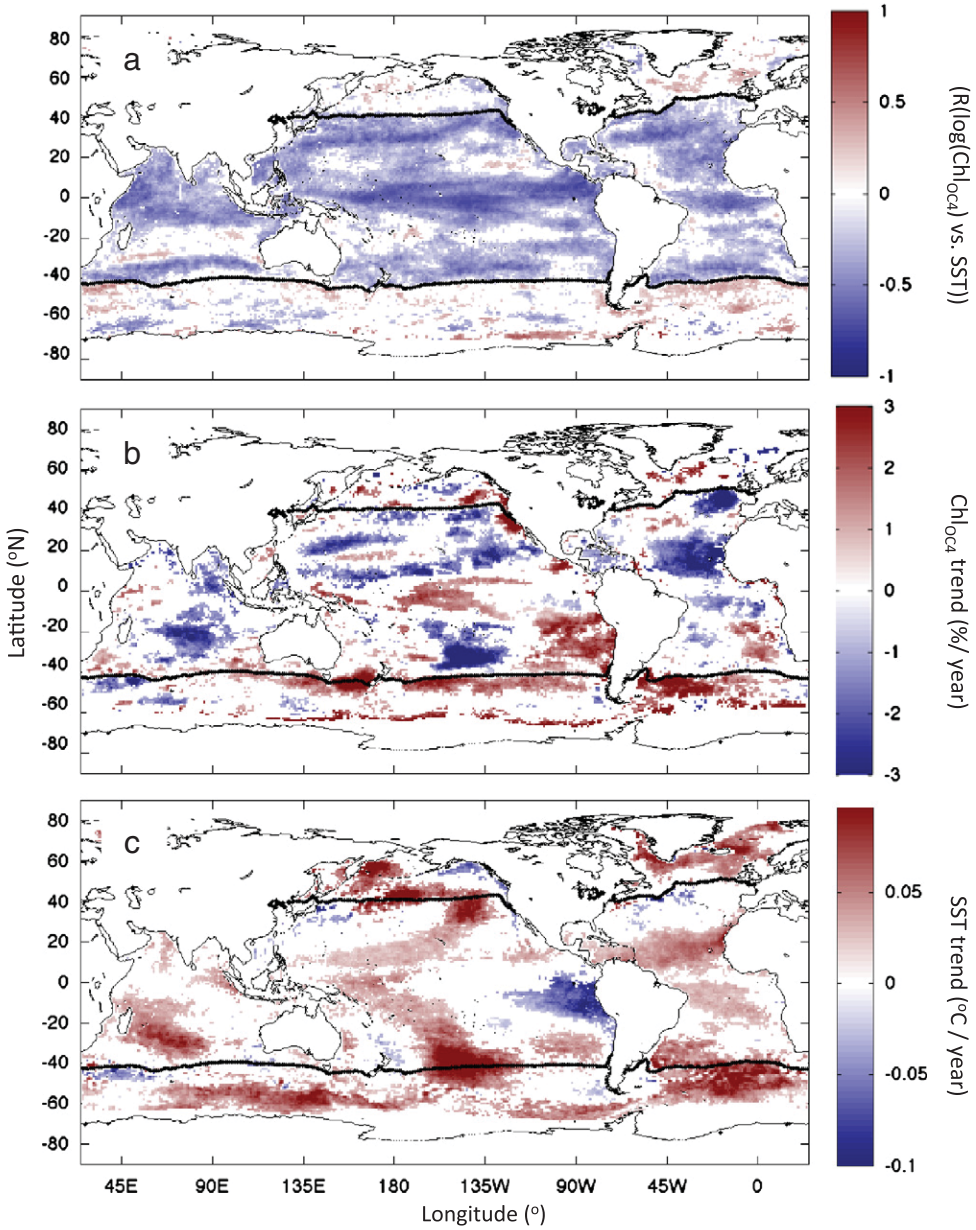

Fig. 4. Regional-scale spatial patterns in the relationship between log(Chl$_{OC4}$) and SST and their trends over time. a) Values of the regression coefficient (R) between log(Chl$_{OC4}$) and SST, b) linear ln(Chl$_{OC4}$) trend (in % year^{-1}) and c) linear SST trend (in °C year^{-1}). Trends are calculated over the entire SeaWiFS mission duration. Statistics calculated for each 1° latitude-longitude bin. Only significant (at the 95% c.i.) correlation or trend determinations are plotted. The mean SST = 15 °C isotherm is shown as the black lines in each panel. This is an update of figure 3.38 from Siegel et al. (2011) using the 2010.0 version of the SeaWiFS data set and the AVHRR Pathfinder v5.2 data set.

patterns seen between Chl$_{OC4}$ and SST (Fig. 4a). The dominant pattern in the warm stratified ocean is an extensive inverse correlation between Chl$_{GSM}$ and SST anomalies particularly in the tropical oceans and for the northern boundary of the subtropical gyres while correlation values are much less coherent in for the cool NH and SH waters (Fig. 7a). As with Chl$_{OC4}$, linear trends of log(Chl$_{GSM}$) over the SeaWiFS record show large areas of both increasing (red areas in Fig. 7b) and decreasing (blue areas) values.

The distribution of the mission-long temporal trends for log(CDM) (Fig. 7c) shows many of the same spatial patterns as seen for log(Chl$_{OC4}$) and log(Chl$_{GSM}$) (Figs. 4b and 7b). However the spatial patterns for log(CDM) trends show more extensive regions of decreasing values compared with both chlorophyll indices supporting the global scale aggregate results (Table 3). The correlations between the log(Chl$_{GSM}$) and log(CDM) regional trends are very strong over the entire domain ($R^2 = 0.650$; $p < 0.001$).

3.4. Roles of physiology vs. biomass accumulation in regulating chlorophyll variability

The large-scale distribution of phytoplankton chlorophyll concentration reflects largely patterns in nutrient supply and thereby differences in phytoplankton abundances (Fig. 1). Phytoplankton can also adjust their intracellular chlorophyll concentrations in response to their light and nutrient environs (e.g., Behrenfeld et al., 2002, 2005; Laws & Bannister, 1980). An important question is how much of the phytoplankton chlorophyll variability (Fig. 8a) is reflective of changes in phytoplankton biomass versus cellular chlorophyll changes in response to light (e.g., Behrenfeld et al., 2002, 2005, 2008; Siegel et al., 2005a; Westberry et al., 2008). To address this question, we statistically partition the variability in the GSM retrieved chlorophyll concentrations (Fig. 8a) using remote sensing proxies for phytoplankton biomass and the chlorophyll to carbon ratio. The GSM-retrieved BBP estimate is

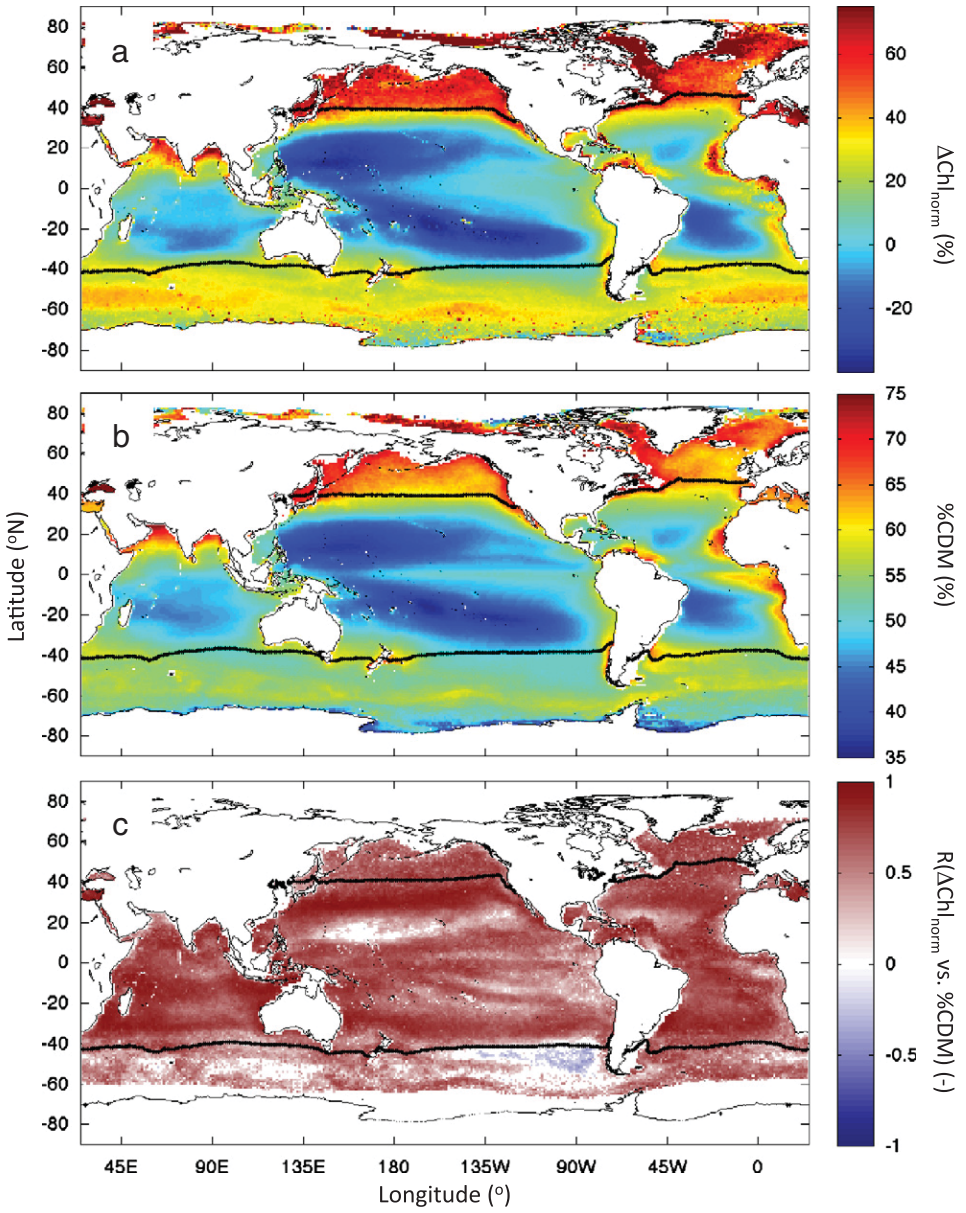

Fig. 5. The importance of CDM on retrieval phytoplankton chlorophyll retrievals from satellite ocean color observations. a) The mission mean normalized chlorophyll concentration anomaly, ΔChl_{norm}. Values of ΔChl_{norm} are calculated as the normalized difference between Chl_{OC4} and Chl_{GSM} ($\Delta Chl_{norm} = 100 * (Chl_{OC4} - Chl_{GSM}) / Chl_{GSM}$; Siegel et al., 2005b). b) The mission mean fraction of non-water light absorption at 443 nm that can be attributed to CDM, %CDM (Siegel et al., 2005b). Values of %CDM are calculated as $100 * CDM / (CDM + a_{ph}(440;Chl_{GSM}))$ where $a_{ph}(440;Chl_{GSM}) = 0.0378\ (Chl_{GSM})^{0.627}$ (Bricaud et al., 1998). The Bricaud et al. (1998) $a_{ph}(440)$ model is used in the %CDM definition because the GSM model was constructed to estimate values of Chl_{GSM} and not $a_{ph}(440)$ (Maritorena et al., 2002). c) The regional-scale distribution of the correlation coefficient (R) for the relationship between ΔChl_{norm} and %CDM. Only significant (at the 95% c.i.) correlation values are plotted. The mean SST = 15 °C isotherm is shown as the black lines. This updates figures from Siegel et al. (2005a) and Siegel et al. (2005b) using the 2010.0 version of the SeaWiFS data set.

used to account for changes in phytoplankton biomass (Section 2.3). Changes in the regional chlorophyll to carbon ratios due to changing light conditions are modeled as $\exp(-3\ I_g)$, where I_g is the median growth irradiance of the mixed layer (Section 2.4). The photoacclimation term used ($\exp(-3\ I_g)$) was originally derived from field measurements from the Atlantic Ocean (Behrenfeld et al., 2002). It was later shown by Behrenfeld et al. (2005) to effectively account for satellite-observed regional relationships between I_g and chlorophyll to carbon ratios. Further, Westberry et al. (2008) reported the same photoacclimation response for nutrient-replete phytoplankton populations using global satellite data. These findings support this parameterization of the photoacclimation response, but further validation is needed and will require routine field measurements of phytoplankton carbon and chlorophyll (e.g., Graff et al., 2012). The impact of the photoacclimation response on chlorophyll concentrations is therefore the product of $\exp(-3\ I_g)$ and BBP and the variability in Chl_{GSM} can be modeled as

$$Chl_{GSM} = f_{bio}BBP + f_{phys}BBP\ \exp\left(-3\ I_g\right)\Big) \quad (1)$$

where f_{bio} and f_{phys} are regression coefficients that quantify the relative importance of biomass and photoacclimation changes on variations of the satellite sensed chlorophyll concentration. All terms in Eq. (1) are standardized (i.e., zero mean, unit variance) so the derived linear regression coefficient values provide, for each regional (1°) bin, a quantification of the relative contributions made by the two processes.

The global distribution of f_{bio} (Fig. 8b) shows dominance (i.e., elevated values ≥ 0.7) throughout the high latitude oceans (poleward of the 15 °C

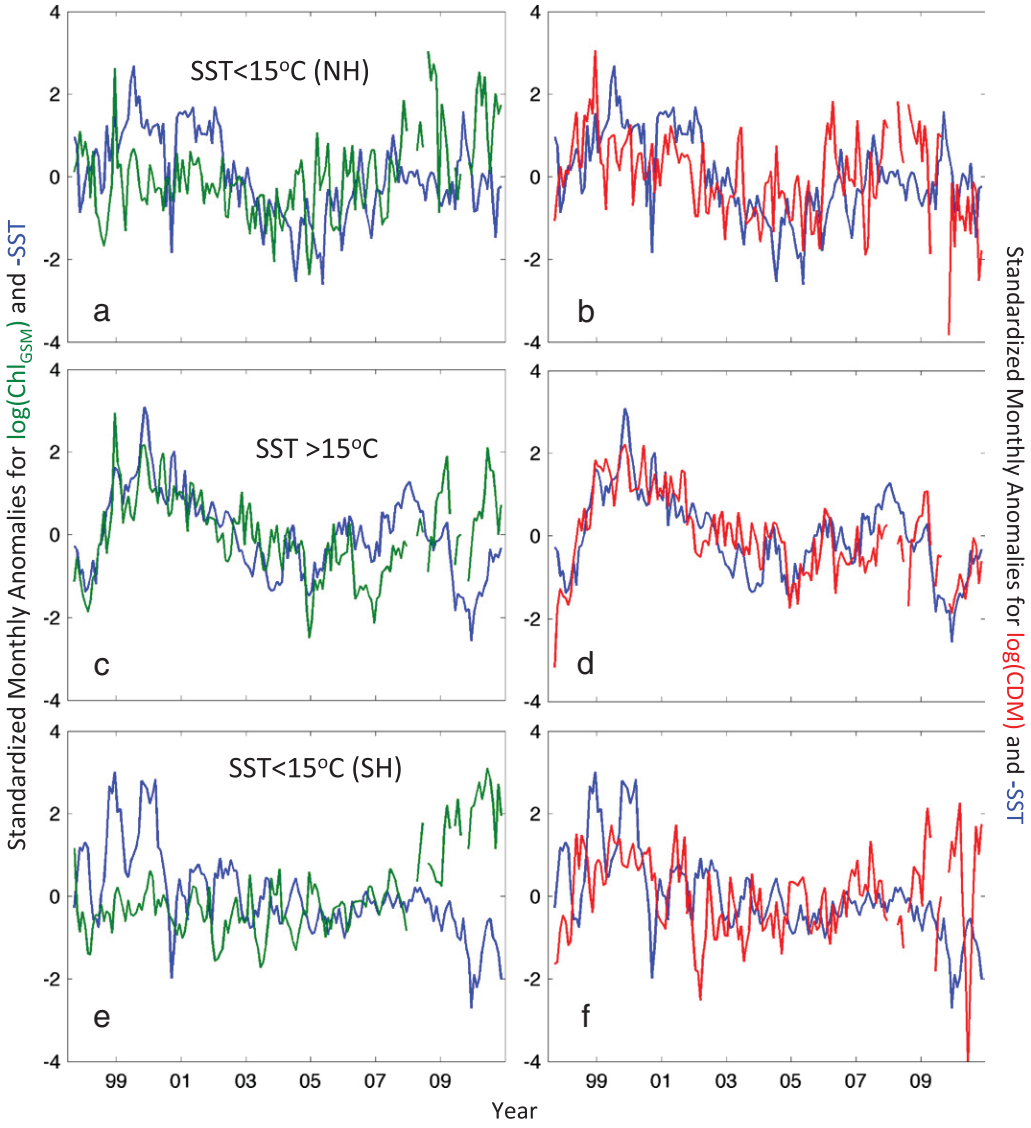

Fig. 6. Relationships between Chl_{GSM} and CDM standardized monthly anomalies (z-scores) with changes in sea surface temperature (SST) for three global regions delineated by the mean SST isotherm. The top panels show the cool (mean SST < 15 °C) northern hemisphere (NH) aggregate for a) log(Chl_{GSM}) and b) log(CDOM). The middle panels show the warm, permanently-stratified ocean aggregate (mean SST > 15 °C) for c) log(Chl_{GSM}) and d) log(CDOM). The lower panels show the cool southern hemisphere (SH) (mean SST < 15 °C for e) log(Chl_{GSM}) and f) log(CDOM). Anomalies are constructed by first removing the monthly mean value for each 1 degree bin of each property and then aggregating the regional, monthly anomalies into global aggregates. Statistics of the correlations between the log(Chl_{GSM}) and log(CDOM) anomalies and the SST anomalies are given in Table 2 and mission length trend analyses are presented in Table 3.

SST isotherm) and in areas of large-scale, persistent or seasonal upwelling (e.g., eastern equatorial Pacific, eastern boundary currents, Arabian Sea, etc.). These are the ocean regions where phytoplankton biomass changes covary with chlorophyll variability. For these regions changes in remote sensed chlorophyll concentrations will be a good proxy for assessing changes in phytoplankton biomass. However throughout much of the subtropical ocean, f_{phys} dominates chlorophyll variability (Fig. 8c). High values of f_{phys} are also found in the central tropical Pacific Ocean and in the Mediterranean Sea. These broad red areas in Fig. 8c correspond to regions where phytoplankton physiological responses to seasonal changes in light are the dominant cause of surface chlorophyll variability. In some areas where f_{phys} is dominant (>0.5), retrieved values of f_{bio} are negative (blue areas in Fig. 8b; e.g., western north Pacific and South Atlantic and South Pacific Subtropical Gyres). An inverse relationship between Chl_{GSM} and phytoplankton biomass was also found in many of the same regions of the world's oceans (see figure 2 of Behrenfeld et al., 2005). There are also broad regions of the ocean where the regression coefficients are not significantly different from zero (white areas in Figs. 8b and 8c). These regions largely coincide in regions where there is little variability in chlorophyll concentrations (Fig. 8a). The proxies for phytoplankton carbon concentration and the chlorophyll to carbon ratio used in this analysis are at a nascent stage of development. Yet they demonstrate that satellite-retrieved chlorophyll concentrations contain information about changes in both phytoplankton biomass and its physiological state and that chlorophyll concentrations alone are often an inappropriate proxy for phytoplankton abundance variations.

4. Discussion and conclusions

Our analysis of regional- to global-scale phytoplankton dynamics using SeaWiFS ocean color observations illustrates several important results about the interpretation of changes in phytoplankton properties assessed from satellite ocean color observations. First, the global ocean biosphere is too complex to be described by a single index, such as chlorophyll concentration. Second, this complexity has important bearings on how climate-relevant trends in the ocean biosphere are assessed. Third, the simple comparison of global and regional scale trends illustrates the difficulty in extrapolating from the time series sampling of a

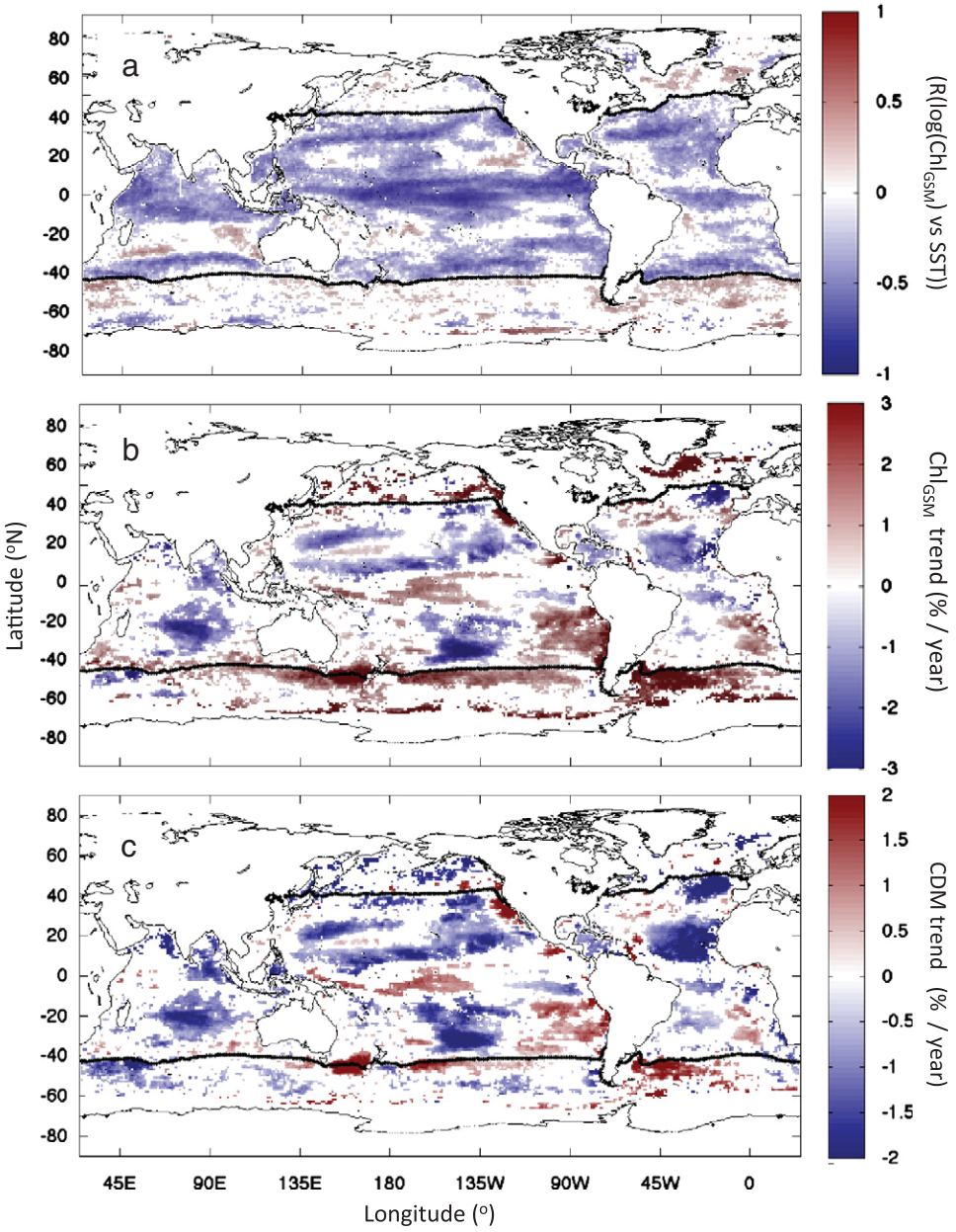

Fig. 7. Regional-scale spatial patterns in the relationship between log(Chl_{GSM}) and SST and the trends in log(Chl_{GSM}) over time. a) Values of the regression coefficient (R) between log(Chl_{GSM}) and SST, b) linear log(Chl_{GSM}) trend (in % $year^{-1}$) and c) linear log(CDM) trend (in % $year^{-1}$). Trends are calculated over the entire SeaWiFS mission duration. Statistics calculated for each 1° latitude-longitude bin. Only significant (at the 95% c.i.) correlation or trend determinations are plotted. The mean SST = 15 °C isotherm is shown as the black lines in each panel.

relatively few locations to estimate global trends. Last, the SeaWiFS mission provided a stable and traceable source of ocean remote sensing reflectance spectra, which were critical for correctly analyzing temporal changes in global phytoplankton dynamics presented here. In the following, we discuss 1) the temporal trends in the ocean biosphere found on regional to global scales from the SeaWiFS mission and their implications for the assessment of trends on decadal to centennial time scales, 2) future approaches to the remote sensing of phytoplankton dynamics in a complex ocean, and 3) reflections for how the SeaWiFS mission provides a path for addressing these challenges in the future.

4.1. Global ocean biosphere trends over the SeaWiFS era and beyond

The present findings highlight several important points concerning the assessment of long-term trends from satellite ocean color observations. First, variability in the three global aggregates was dominated by ocean climate variations on interannual time scales and not by long-term trends over the 13-year lifespan of SeaWiFS. The strong correspondence between monthly anomalies in SST and Chl_{OC4} (and other properties) demonstrates the close interrelationship between ocean biology and climate variations (Table 2; Figs. 3 & 6). In addition to these dominant seasonal-to-interannual variations, significant 13-year linear trends are found (Table 3). These long-term trends, however, explain very little of the total observed variations. For example, the most significant statistically linear trend found for the warm ocean aggregate explained only ~19% of the observed variance (for log(CDOM); Fig. 6d; Table 3). It seems likely that a linear trend applied over a single satellite mission will be too short to properly assess long-term temporal trends in the global ocean biosphere (e.g., Henson et al., 2010; Vantrepotte & Mélin, 2011).

The present results also provide information about the spatial scales for decadal trends in the global biosphere. A comparison of

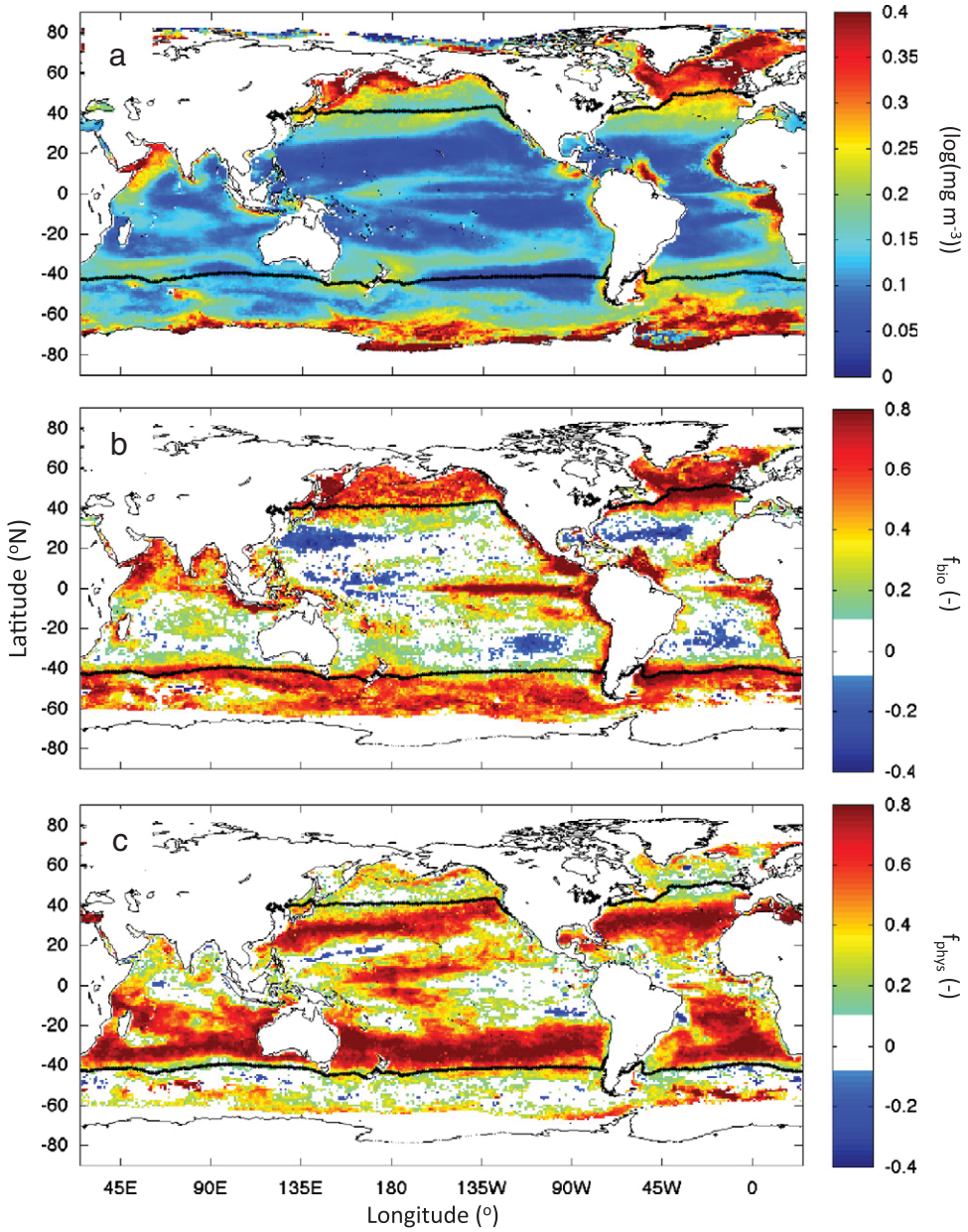

Fig. 8. Chlorophyll variability and its relation to biomass and light-induced physiological changes. a) Standard deviation in log(Chl_{GSM}) estimated over the SeaWiFS mission. b) Standardized regression slopes for predicting Chl_{GSM} as function of changes in biomass (f_{bio} in Eq. 1) and c) and for changes in rates of photoacclimation (f_{phys}). Values of the standardized regression slopes near one indicate the dominance of that process on Chl_{GSM} variability. Details of model configuration are provided in the text. Only statistically significant (95% c.i.) slope values are shown. The mean SST = 15 °C isotherm is shown as the black lines in each panel.

the global (Fig. 3) and regional scale trends (Figs. 4b) illustrates the difficulty in extrapolating from in situ sampling of a relatively few locations to estimate global scale trends. Fixed-location time-series measurement programs, such as the Bermuda Atlantic Time series Station (BATS) and the Hawaii Ocean Time-series (HOT), are critical observatories of the processes driving changes in ocean biosphere. However, long-term trends derived from them provide at best a single-point in a map like Fig. 4b. Clearly, data from many long-term monitoring sites – sampling both areas of increasing and decreasing trends – are needed to create a global assessment of change.

The trends diagnosed here show both similarities and differences with previous studies of temporal trends found using SeaWiFS observations. For example, Gregg et al. (2005) find a ~4% increase in global chlorophyll concentrations over the first six years of the SeaWiFS record (1998 to 2003), with the highest increases in coastal environments. Contrasting this, Behrenfeld and Boss (2006) find decreasing levels of global chlorophyll concentrations and rates of net primary production (NPP; from 1999 to 2005) that follow strong increases in both Chl_{OC4} and NPP during the transition in 1998 from El Niño to La Nina conditions. Vantrepotte and Mélin (2009) examine the first ten years of the SeaWiFS record and find trends for biogeochemical provinces consistent with the present analysis, which is expected considering the similarity in the periods studied. Methodology is likely to be important as well. The present study log-transforms the chlorophyll observations before global scale anomalies are calculated while the Gregg et al. (2005) study does not. Not assuming log-normality will likely amplify the influence of the fewer, highly productive sites in global summaries. Thus, record length, time period and assumptions in data analysis will all have important roles in quantifying trends.

Evaluating changes on time scales longer than a single mission requires the merging of data across multiple satellite platforms and/or the inclusion of historical field observations. Several researchers

have link data from the Coastal Zone Color Scanner (CZCS) (1978–1985) with the SeaWiFS data record (e.g., Antoine et al., 2005; Gregg et al., 2003; Martinez et al., 2009). Gregg et al., 2003 find a global decline of NPP of more than 6% between CZCS observations in the early 1980s and the first five years of the SeaWiFS record, with most of the decreases occurring at high latitudes. Contrasting these results, Antoine et al. (2005) find a ~22% increase in global chlorophyll concentrations, where most of these increases are due to changes at low latitudes. These two analyses are based on fundamentally different satellite data processing approaches and underscore the importance of consistency of data processing and radiometric calibration standards across multiple missions (McClain, 2009; National Research Council, 2011; Siegel & Franz, 2010).

Only field observations can currently be used to examine trends of global chlorophyll concentrations on longer time scales. Recently Boyce et al. (2010) created a centennial-scale time series of ocean chlorophyll concentrations using both discrete measurements of near-surface chlorophyll concentrations and Secchi disk depth (a measure of water clarity). Using this synthesized data set, Boyce et al. (2010) found an overall chlorophyll decrease over the past century of ~1% per year (and decreasing trends were found for 6 of their 8 global sub-regions). This implies that over the past 100 years there has been a ~63% decrease in global chlorophyll concentrations, which we deem unlikely. The present analysis shows a significant decrease in Chl_{OC4} only for the warm ocean aggregate and decrease was a factor of five smaller than the Boyce et al.'s result (Table 3). Further, significant increases in Chl_{OC4} are found for the two cold ocean aggregates. The satellite data sets discussed here and the Boyce et al.'s (2010) analysis are based on very different methods and do not evaluate the same period of time. However the estimation of a 1% annual global decrease in chlorophyll concentrations is also inconsistent with the fact that the rate of global SST warming has been greater over the past three decades than earlier in the past century (Rayner et al., 2003; Xue et al., 2011).

Resolution of the validity of Boyce et al.'s, (2010) conclusions is beyond the scope of this contribution, although the present discussion provides some useful insights. We note that in response to published comments on their original paper, Boyce et al. (2011) state that "… our statistical models reproduced with high fidelity the well-known seasonal cycles of Chl in different regions and demonstrated clear coherence between Chl and leading climate indicators." Existing satellite ocean color observations have proven quite capable to assess seasonal variations (e.g., Siegel et al., 2002a; Yoder et al., 1993) and responses to climate oscillations (e.g., Behrenfeld et al., 2006; Martinez et al., 2009). However the robust quantification of multi-decadal trends from these data sets has proven to be difficult at best as demonstrated by the strikingly different conclusions drawn by different analysts using the exact same data (e.g., Antoine et al., 2005; Gregg et al., 2003). We speculate that similar issues may be affecting the Boyce et al.'s (2010) analysis where their trends may be retrieved improperly due to the dominance of the larger seasonal and climate oscillation signals and inherent noise in their synthesized data set. A likely source of noise in the Boyce et al.'s (2010) data set is the lack of uniformity (and statistical independence) of available historic observations of the global ocean (see Fig. 1 of Boyce et al., 2010) as compared to the expected spatial scales of long-term trends (Figs. 4b & 7b). Further research is needed to better understand the role of sampling on the centennial-scale trends estimated by Boyce et al. (2010).

This discussion raises several important points about the quantification of long-term trends of the global biosphere. A thirteen-year mission is a short amount of time to detect and quantify trends in the global ocean biological properties and small details in periods chosen and/or analysis periods can impact the trends diagnosed. Longer time series require multiple satellite missions and the creation and maintenance of a multi-satellite ocean color time series will require the careful bridging between existing and planned missions, including the tracking of appropriate reflectance targets such as the moon and the multiple reprocessing of available data sets (e.g., McClain, 2009; National Research Council, 2011; Siegel & Franz, 2010). The development of a multi-satellite ocean color time series remains the most feasible approach for documenting regional- to global-scale variability of the ocean biosphere (National Research Council, 2011). The present analysis also provides context for evaluating the suitability of historical observations for detecting long-term trends in the global biosphere.

4.2. Remote sensing of an optically complex ocean

A major point of this paper is to show that the dynamics of the open ocean ecosystems are simply too complex to be described by a single index, such as chlorophyll concentration. Understanding this complexity requires quantifying the variability in relevant ocean color constituents, such as chlorophyll, phytoplankton carbon and CDOM, and their responses to perturbations in the physical ocean environment. Further additional factors not considered here, such as the phytoplankton community composition and particle size distribution, need to be assessed in the future to understand the role of phytoplankton dynamics in regulating important biogeochemical factors, including carbon export and net community production.

The optically complex ocean has implications for the interpretation of long-term trends in global phytoplankton chlorophyll observations. For example, the warm ocean aggregate trends for CDM and Chl_{OC4} decrease significantly over time while the linear trend for Chl_{GSM} vs. time is statistically insignificant (Table 3). Also as shown previously, there is a strong correspondence between CDM and Chl_{OC4} where increases in %CDM create an overestimate of band-ratio retrieved values of chlorophyll concentrations (Fig. 5c). Both lines of evidence indicate that the observed trend in Chl_{OC4} for the warm aggregate ocean is likely due to changes in CDOM, which dominates the CDM signal, and not phytoplankton chlorophyll concentrations.

This uncertainty in the assessment of long-term trends in ocean biosphere points to the importance of understanding the cycling of open ocean CDOM (e.g., Nelson & Siegel, 2002, 2013). The seasonal dynamics of surface CDOM are thought to be controlled by the same physical forcings that regulate chlorophyll concentrations; namely the seasonal mixing of subsurface CDOM stocks and net CDOM production during the spring phytoplankton bloom followed by photobleaching of mixed layer CDOM stocks in the summer and a regeneration of CDOM in the lower euphotic zone (e.g., Nelson & Siegel, 2013; Nelson et al., 1998; Siegel et al., 2002b). However CDOM is comprised of a suite of chromophores and changes in CDOM will occur on a multitude of time scales from the time course of an uptake experiment in the laboratory to the multi-decadal time scale of cycling in the deep ocean (e.g., Kitidis et al., 2006; Nelson & Siegel, 2002, 2013; Nelson et al., 2004, 2010; Swan et al., 2009, 2012; Yamashita & Tanoue, 2009). A quantitative description of CDOM dynamics is sorely needed, but this has yet to be developed. CDOM is important in its own rights, as it has a dominant role in solar light absorption (Fig. 1) and its variability helps regulate many biogeochemical processes (e.g., Millet et al., 2010; Toole et al., 2008; Zepp et al., 2007).

There are also physiological complexities to the global ocean biosphere. We have shown that in highly productive regions where blooms are common, changes in chlorophyll concentration are dominated by changes in phytoplankton biomass. However throughout much of the subtropical oceans, chlorophyll variations provide information primarily on physiological responses to light (and nutrients) and not changes to biomass (Fig. 8c). This means that remote sensing retrievals of chlorophyll are not always a good proxy for phytoplankton concentrations. The present analysis of biomass variability is based on BBP determinations (Behrenfeld et al., 2005, 2008; Westberry et al., 2008). Improvements to this method require global in situ observations of phytoplankton biomass, which are presently lacking. Clearly, routine determinations of phytoplankton carbon concentration are the first step

towards developing better methods for assessing phytoplankton carbon from satellite observations (e.g., Graff et al., 2012).

Advances are also needed to assess changes in phytoplankton community structure from satellite observations (e.g., Dierssen, 2010). Assessments of phytoplankton community structure have been made by either diagnosing phytoplankton functional type or phytoplankton size class (e.g., Alvain et al., 2005; Brewin et al., 2011; Bricaud et al., 2012; Kostadinov et al., 2010; Mouw & Yoder, 2010). Again, available field data sets remain a major limitation and currently only chemotaxonomic analysis of phytoplankton pigment concentrations or particle size distribution determinations are used as "ground truth". Both approaches are limited in their ability to diagnose phytoplankton community structure information (e.g., Higgins et al., 2011; Kostadinov et al., 2010) and this is another area where advances in field methodologies are needed.

Progress in understanding the optically complex ocean requires improvements and expansion of field data sets to develop and test bio-optical algorithms as well as advancements in space technology. All ocean color algorithms are empirical and the availability of high quality observations that span the application space for these algorithms is central for these developments. Many suggestions for improvements in field data needed for bio-optical model development have been made already. One important suggestion is refining the quality of existing data sets, such as NOMADv2, which will enable researchers to choose the highest quality or most extensive observations to develop and test their models.

Improvements in space hardware are also needed to best account for the complex ocean environment. Successful atmospheric correction is a critical part of satellite ocean color remote sensing (see Section 2.1). This gets harder as several important oceanic and atmospheric constituents, such as CDOM and absorbing aerosol concentrations, have similar optical signatures yet they need to be eliminated to prevent spurious interpretations of phytoplankton dynamics (e.g., Gordon, 1997). Additional ocean color bands in the near-ultraviolet portion of the spectrum would help separate CDOM from phytoplankton absorption and will assist in characterizing absorbing aerosol loads, as both of these optical properties strongly absorb in the near-UV. Another area where improvements in space-based hardware could be useful is the assessment of phytoplankton community structure. High spectral resolution satellite observations (~5 nm) are a very promising technique that can be used to distinguish the contributions of individual phytoplankton pigment concentrations (e.g., Bidigare et al., 1989; Bracher et al., 2009; Torrecilla et al., 2011). Many of these suggestions have been incorporated in the planning document for the Pre-Aerosol, Clouds, and ocean Ecosystem (PACE) Mission Science Definition Team (PACE SDT, 2012) as well as several other international satellite ocean color mission plans.

4.3. SeaWiFS legacy and its use as a periscope to the future

The SeaWiFS mission provided the first consistent, long-term, well-sampled and stable estimates of ocean remote sensing reflectance spectra and these observations were central for the analysis of temporal changes in regional to global phytoplankton dynamics presented here. The loss of the SeaWiFS data stream marks the end of an observational time-series largely free of instrument artifacts and a critical record against which other satellite ocean color sensors have been made useful (e.g., Jeong et al., 2011; Kwiatkowska et al., 2008; Meister et al., 2012). Establishing a quality replacement for SeaWiFS that will sustain, as well as advance, the ocean color time series is of paramount importance (National Research Council, 2011; Siegel & Franz, 2010).

Results of the present study also provide unique insights for future satellite ocean color mission capabilities. First as concluded above, measurements of ocean remote sensing reflectance spectra need to be sustained over a long time (>10 years) and be traceable to known standards. Temporal changes of the ocean biosphere, particularly trends, can only be evaluated knowing the quality of the underlying data set. This requires a vicarious calibration capability including appropriate field sampling and an independent assessment of satellite instrument stability, such as would be available from lunar viewing. This will enable the setting of satellite gains and characteristics as a function of time. It is important that this capability be in place beyond the planned mission lifetime so records from multiple missions can be stitched together to make the multi-decadal data sets needed.

This discussion bears consideration of what is meant by a "satellite mission", which should be more than just the hardware and software required to make a measurement from space. Many of the points made in the discussion so far, such as the need for vicarious calibration, field data for model development, and sequential reprocessing of the data stream beyond the lifetime of a mission, suggest that an integrated approach is required. Furthermore many of the questions and problems, including the assessments of phytoplankton physiological state, carbon export, net community production, air-sea CO_2 exchanges, all require the integration of satellite observations with Earth system models and the use of detailed laboratory investigations that guide the development of these models. Hence, we suggest that the development of a "satellite mission" includes all aspects of the mission required to answer the science questions that motivated its implementation in orbit.

SeaWiFS was unique as it created a blueprint for how ocean biosphere observations should be made on decadal time scales (National Research Council, 2011). As reported here, analysis of the SeaWiFS observations also provides directions for future satellite ocean color observations. These advanced observational tools will likely enable new discoveries of the structure and functioning of ocean ecosystems, which will in turn lead to improved understanding of our oceans and their wise stewardship.

Acknowledgments

The authors would like to acknowledge the NASA Ocean Biology and Biogeochemistry program for its long-term support of satellite ocean color research and the Orbital Sciences Corporation and GeoEye who were responsible for the launch, satellite integration and on-orbit management the SeaWiFS mission. The authors would also like to thank the anonymous reviewers for their excellent and extremely helpful comments on our manuscript.

Appendix A. Supplementary data

Supplementary information to this article can be found online at http://dx.doi.org/10.1016/j.rse.2013.03.025.

References

Alvain, S., Moulin, C., Dandonneau, Y., & Bréon, F. M. (2005). Remote sensing of phytoplankton groups in case 1 waters from global SeaWiFS imagery. *Deep-Sea Research Part I*, *52*, 1989–2004.

Antoine, D., Morel, A., Gordon, H. R., Banzon, V. F., & Evans, R. H. (2005). Bridging ocean color observations of the 1980s and 2000s in search of long-term trends. *Journal of Geophysical Research*, *110*. http://dx.doi.org/10.1029/2004JC002620 (C06009).

Antoine, D., Siegel, D. A., Kostadinov, T., Maritorena, S., Nelson, N. B., Gentili, B., et al. (2011). Variability in optical particle backscattering in contrasting bio-optical oceanic regimes. *Limnology and Oceanography*, *56*, 955–973.

Bailey, S. W., & Werdell, P. J. (2006). A multi-sensor approach for the on-orbit validation of ocean color satellite data products. *Remote Sensing of Environment*, *102*, 12–23.

Balch, W. M., Drapeau, D. T., Bowler, B. C., Lyczskowski, E., Booth, E. S., & Alley, D. (2011). The contribution of coccolithophores to the optical and inorganic carbon budgets during the Southern Ocean Gas Exchange Experiment: New evidence in support of the "Great Calcite Belt" hypothesis. *Journal of Geophysical Research*, *116*. http://dx.doi.org/10.1029/2011JC006941.

Behrenfeld, M. J. (2010). Abandoning Sverdrup's critical depth hypothesis on phytoplankton blooms. *Ecology*, *91*, 977–989.

Behrenfeld, M. J., & Boss, E. (2003). The beam attenuation to chlorophyll ratio: An optical index of phytoplankton photoacclimation in the surface ocean? *Deep-Sea Research Part I*, *50*, 1537–1549.

Behrenfeld, M. J., & Boss, E. (2006). Beam attenuation to chlorophyll concentration as alternative indices of phytoplankton biomass. *Journal of Marine Research*, *64*, 431–451.

Behrenfeld, M. J., Boss, E., Siegel, D. A., & Shea, D. M. (2005). Carbon-based ocean productivity and phytoplankton physiology from space. *Global Biogeochemical Cycles*, *19*. http://dx.doi.org/10.1029/2004GB002299.

Behrenfeld, M. J., Halsey, K., & Milligan, A. (2008). Evolved physiological responses of phytoplankton to their integrated growth environment. *Proceedings of the Royal Society B: Biological Sciences*, *363*. http://dx.doi.org/10.1098/rstb.2008.0019.

Behrenfeld, M. J., Marañón, E., Siegel, D. A., & Hooker, S. B. (2002). Photoacclimation and nutrient-based model of light-saturated photosynthesis for quantifying oceanic primary production. *Marine Ecology Progress Series*, *228*, 103–117.

Behrenfeld, M. J., O'Malley, R. T., Siegel, D. A., McClain, C. R., Sarmiento, J. L., Feldman, G. C., et al. (2006). Climate-driven trends in contemporary ocean productivity. *Nature*, *444*, 752–755.

Behrenfeld, M. J., Randerson, J. T., McClain, C. R., Feldman, G. C., Sietse, O. L., Tucker, C. J., et al. (2001). Biospheric primary production during an ENSO transition. *Science*, *291*, 2594–2597.

Bidigare, R., Morrow, J., & Kiefer, D. (1989). Derivative analysis of spectral absorption by photosynthetic pigments in the western Sargasso Sea. *Journal of Marine Research*, *47*, 323–341.

Bishop, J. K. B., Davis, R. E., & Sherman, J. T. (2002). Robotic observations of dust storm enhancement of carbon biomass in the North Pacific. *Science*, *298*, 817–821.

Boyce, D. G., Lewis, M. L., & Worm, B. (2010). Global phytoplankton decline over the past century. *Nature*, *466*, 591–596.

Boyce, D. G., Lewis, M. L., & Worm, B. (2011). Is there a decline in marine phytoplankton? Reply. *Nature*, *472*, E8–E9. http://dx.doi.org/10.1038/nature09953.

Bracher, A., Vountas, M., Dinter, T., Burrows, J. P., Röttgers, R., & Peeken, I. (2009). Quantitative observation of cyanobacteria and diatoms from space using PhytoDOAS on SCIAMACHY data. *Biogeosciences*, *6*, 751–764.

Brewin, R. J. W., Hartman-Mountford, N. J., Lavender, S. J., Raitsos, D. E., Hirata, T., Uitz, J., et al. (2011). An intercomparison of bio-optical techniques for detecting dominant phytoplankton size class from satellite remote sensing. *Remote Sensing of Environment*, *115*, 325–339.

Bricaud, A., Ciotti, A. M., & Gentili, B. (2012). Spatial-temporal variations in phytoplankton size and colored detrital matter absorption at global and regional scales, as derived from twelve years of SeaWiFS data (1998–2009). *Global Biogeochemical Cycles*, *26*. http://dx.doi.org/10.1029/2010GB003952.

Bricaud, A., Claustre, H., Ras, J., & Oubelkheir, K. (2004). Natural variability of phytoplankton absorption in oceanic waters: Influence of the size structure of algal populations. *Journal of Geophysical Research*, *109*. http://dx.doi.org/10.1029/2004JC002419 C11010.

Bricaud, A., Morel, A., Babin, M., Allali, K., & Claustre, H. (1998). Variations of light absorption by suspended particles with the chlorophyll *a* concentration in oceanic (case 1) waters: Analysis and implications for bio-optical models. *Journal of Geophysical Research*, *103*, 31,033–31,044.

Campbell, J. W. (1995). The lognormal distribution as a model for bio-optical variability in the sea. *Journal of Geophysical Research*, *100*, 13237–13254.

Ciotti, A. M., Lewis, M. R., & Cullen, J. J. (2002). Assessment of the relationships between dominant cell size in natural phytoplankton communities and the spectral shape of the absorption coefficient. *Limnology and Oceanography*, *47*, 404–417.

Clancy, R. M., & Sadler, W. D. (1992). The fleet numerical oceanography center suite of oceanographic models and products. *Weather and Forecasting*, *7*, 307–327.

Dall'Olmo, G., Westberry, T. K., Behrenfeld, M. J., Boss, E., & Slade, W. H. (2009). Significant contribution of large particles to optical backscattering in the open ocean. *Biogeosciences*, *6*, 947–967.

Dall'Olmo, G., Boss, E., Behrenfeld, M. J., Westberry, T. K., Courties, C., Prieur, L., et al. (2011). Inferring phytoplankton carbon and eco-physiological rates from diel cycles of spectral particulate beam-attenuation coefficient. *Biogeosciences*, *8*, 3423–3439.

Dierssen, H. M. (2010). Perspectives on empirical approaches for ocean color remote sensing of chlorophyll in a changing climate. *Proceedings of the National Academy of Sciences of the United States of America*, *107*, 17073–17078.

Doney, S. C. (2006). Oceanography: Plankton in a warmer world. *Nature*, *444*, 695–696.

DuRand, M. D., & Olson, R. J. (1996). Contributions of phytoplankton light scattering and cell concentration changes to diel variations in beam attenuation in the equatorial Pacific from flow cytometric measurements of pico-, ultra-, and nanoplankton. *Deep-Sea Research Part II*, *43*, 891–906.

Eplee, R. E., Jr., Meister, G., Patt, F. S., Franz, B. A., & McClain, C. R. (2011). Uncertainty assessment of the SeaWiFS on-orbit calibration, in *Earth Observing Systems XVI*. In J. J. Butler, X. Xiong, & X. Gu (Eds.), *Proc. SPIE*, *8153*. (pp. 815310).

Falkowski, P. G. (1984). Physiological responses of phytoplankton to natural light regimes. *Journal of Plankton Research*, *6*, 295–307.

Falkowski, P. G., Barber, R. T., & Smetacek, V. (1998). Biogeochemical controls and feedbacks on ocean primary production. *Science*, *281*, 200–206.

Field, C. B., Behrenfeld, M. J., Randerson, J. T., & Falkowski, P. G. (1998). Primary production of the biosphere: Integrating terrestrial and oceanic components. *Science*, *281*, 237–240.

Franz, B. A., Bailey, S. W., Werdell, P. J., & McClain, C. R. (2007). Sensor-independent approach to vicarious calibration of satellite ocean color radiometry. *Applied Optics*, *46*, 5068–5082.

Gernez, P., Antoine, D., & Huot, Y. (2011). Diel cycles of the particulate beam attenuation coefficient under varying trophic conditions in the northwestern Mediterranean Sea: Observations and modeling. *Limnology and Oceanography*, *56*, 17–36.

Gordon, H. R. (1997). Atmospheric correction of ocean color imagery in the Earth Observing System era. *Journal of Geophysical Research*, *102*, 17081–17106.

Graff, J. R., Milligan, A. J., & Behrenfeld, M. J. (2012). The measurement of phytoplankton biomass using flow-cytometric sorting and elemental analysis of carbon. *Limnology and Oceanography: Methods*, *10*, 910–920.

Green, R. E., Sosik, H. M., Olson, R. J., & DuRand, M. D. (2003). Flow cytometric determination of size and complex refractive index for marine particles: Comparison with independent and bulk estimates. *Applied Optics*, *42*, 526–541.

Gregg, W. W., Casey, N. W., & McClain, C. R. (2005). Recent trends in global ocean chlorophyll. *Geophysical Research Letters*, *32* (L03606).

Gregg, W. W., Conkright, M. E., Ginoux, P., O'Reilly, J. E., & Casey, N. W. (2003). Ocean primary production and climate: Global decadal changes. *Geophysical Research Letters*, *30*, 1809. http://dx.doi.org/10.1029/2003GL016889.

Halsey, K. H., Milligan, A., & Behrenfeld, M. J. (2010). Physiological optimization underlies growth rate-independent chlorophyll-specific gross and net primary production. *Photosynthesis Research*, *103*, 125–137. http://dx.doi.org/10.1007/s11120-009-9526-z.

Henson, S. A., Sarmiento, J. L., Dunne, J. P., Bopp, L., Lima, I., Doney, S. C., et al. (2010). Detection of anthropogenic climate change in satellite records of ocean chlorophyll and productivity. *Biogeosciences*, *7*, 621–640.

Higgins, H. W., Wright, S. W., & Schülter, L. (2011). Quantitative interpretation of chemotaxonomic pigment data. In S. Roy, C. A. Llewellyn, E. S. Egeland, & G. Johnsen (Eds.), *Phytoplankton pigments* (pp. 257–313). : SCOR — Cambridge University Press.

Hu, C., Carder, K. L., & Muller-Karger, F. E. (2001). How precise are SeaWiFS ocean color estimates? Implications of digitization-noise errors. *Remote Sensing of Environment*, *76*, 239–249.

Huot, Y., Morel, A., Twardowski, M. S., Stramski, D., & Reynolds, R. A. (2008). Particle optical backscattering along a chlorophyll gradient in the upper layer of the eastern South Pacific Ocean. *Biogeosciences*, *5*, 495–507.

IOCCG (2006). In ZhongPing Lee (Ed.), *Remote sensing of inherent optical properties: Fundamentals, tests of algorithms, and applications. Report #5* (pp. 126) (http://www.ioccg.org/reports/report5.pdf)

Jeong, M. -J., Hsu, N. C., Kwiatkowska, E. J., Franz, B. A., Meister, G., & Salustro, C. E. (2011). Impacts of cross-platform vicarious calibration on the deep blue aerosol retrievals for moderate resolution imaging spectroradiometer aboard Terra. *Transactions on Geoscience and Remote Sensing*, *40*(12).

Johnson, K. S., Berelson, W. M., Boss, E. S., Chase, Z., Claustre, H., Emerson, S. R., et al. (2009). Observing biogeochemical cycles at global scales with profiling floats and gliders: Prospects for a global array. *Oceanography*, *22*, 216–225.

Kirk, J. T. O. (1994). *Light and photosynthesis in aquatic ecosystems* (2nd ed.). Cambridge, U.K.: Cambridge Univ. Press (509 pp).

Kitidis, V., Stubbins, A., Uher, G., Upstill-Goddard, R., Law, C., & Woodward, E. (2006). Variability of chromophoric organic matter in surface waters of the Atlantic Ocean. *Deep-Sea Research Part II*, *53*, 1666–1684.

Kostadinov, T. S., Siegel, D. A., & Maritorena, S. (2010). Global variability of phytoplankton functional types from space: Assessment via the particle size distribution. *Biogeosciences*, *7*, 3239–3257.

Kwiatkowska, E. J., Franz, B. A., Meister, G., McClain, C., & Xiong, X. (2008). Cross-calibration of ocean-color bands from Moderate Resolution Imaging Spectroradiometer on Terra platform. *Applied Optics*, *47*(36).

Laws, E. A., & Bannister, T. T. (1980). Nutrient- and light-limited growth of *Thalassiosira fluviatilis* in continuous culture, with implications for phytoplankton growth in the ocean. *Limnology and Oceanography*, *25*, 457–473.

Lee, Z. P., Carder, K. L., & Arnone, R. (2002). Deriving inherent optical properties from water color: A multi-band quasi-analytical algorithm for optically deep waters. *Applied Optics*, *41*, 5755–5772.

Lee, Z., Shang, S., Hu, C., Lewis, M., Arnone, R., Li, Y., et al. (2010). Time series of bio-optical properties in a subtropical gyre: Implications for the evaluation of interannual trends of biogeochemical properties. *Journal of Geophysical Research*, *115*. http://dx.doi.org/10.1029/2009JC005865 (C09012).

Maritorena, S., Fanton d'Andon, O. H., Mangin, A., & Siegel, D. A. (2010). Merged satellite ocean color data products using a bio-optical model: Characteristics, benefits and issues. *Remote Sensing of Environment*, *114*, 1791–1804.

Maritorena, S., Siegel, D. A., & Peterson, A. R. (2002). Optimization of a semianalytical ocean color model for global-scale applications. *Applied Optics*, *41*, 2705–2714.

Martinez, E., Antoine, D., D'Ortenzio, F., & Gentili, B. (2009). Climate-driven basin-scale decadal oscillations of oceanic phytoplankton. *Science*, *326*, 1253–1256.

McClain, C. R. (2009). A decade of satellite ocean color observations. *Annual Review of Marine Science*, *1*, 19–42.

McClain, C. R., Feldman, G. C., & Hooker, S. B. (2004). An overview of the SeaWiFS project and strategies for producing a climate research quality global ocean bio-optical time series. *Deep-Sea Research Part II*, *51*, 5–42.

Meister, G., Franz, B. A., Kwiatkowska, E. J., & McClain, C. R. (2012). Corrections to the calibration of MODIS aqua ocean color bands derived from SeaWiFS data. *Transactions on Geoscience and Remote Sensing*, *50*(1).

Millet, D. B., Guenther, A., Siegel, D. A., Nelson, N. B., Singh, H. B., de Gouw, J. A., et al. (2010). Global atmospheric budget of acetaldehyde: 3D model analysis and constraints from in-situ and satellite observations. *Atmospheric Chemistry and Physics*, *10*, 3405–3425.

Morel, A. (1988). Optical modeling of the upper ocean in relation to its biogenous matter content (case 1 water). *Journal of Geophysical Research*, *93*, 10,749–10,768.

Morel, A., & Bricaud, A. (1981). Theoretical results concerning light absorption in a discrete medium, and application to the specific absorption of phytoplankton. *Deep Sea Research*, *28*, 1375–1393.

Morel, A., Claustre, H., & Gentili, B. (2010). The most oligotrophic subtropical zones of the global ocean: Similarities and differences in terms of chlorophyll and yellow substance. *Biogeosciences*, *7*, 3139–3151.

Morel, A., Huot, Y., Gentili, B., Werdell, P., Hooker, S., & Franz, B. (2007). Examining the consistency of products derived from various ocean color sensors in open ocean (case 1) waters in the perspective of a multi-sensor approach. *Remote Sensing of Environment*, *111*, 69–88.

Mouw, C. B., & Yoder, J. A. (2010). Optical determination of phytoplankton size distribution from global SeaWiFS imagery. *Journal of Geophysical Research*, *115*. http://dx.doi.org/10.1029/1020JC006337 (C12018).

National Research Council (2011). *Assessing the requirements for sustained ocean color research and operations*. Washington D.C.: National Academy Press (148 pp).

Nelson, N. B., Carlson, C. A., & Steinberg, D. K. (2004). Production of chromophoric dissolved organic matter by Sargasso Sea microbes. *Marine Chemistry*, *89*, 273–287.

Nelson, N. B., & Siegel, D. A. (2002). Chromophoric DOM in the open ocean. In D. A. Hansell, & C. A. Carlson (Eds.), *Biogeochemistry of marine dissolved organic matter* (pp. 547–578). San Diego, CA: Academic Press.

Nelson, N. B., & Siegel, D. A. (2013). The global distribution and dynamics of chromophoric dissolved organic matter. *Annual Review of Marine Science*, *5*, 447–476.

Nelson, N. B., Siegel, D. A., Carlson, C. A., & Swan, C. M. (2010). Tracing global biogeochemical cycles and meridional overturning circulation using chromophoric dissolved organic matter. *Geophysical Research Letters*, *37*. http://dx.doi.org/10.1029/2009GL042325 (L03610).

Nelson, N. B., Siegel, D. A., Carlson, C. A., Swan, C., Smethie, W. M., Jr., & Khatiwala, S. (2007). Hydrography of chromophoric dissolved organic matter in the North Atlantic. *Deep-Sea Research Part I*, *54*, 710–731.

Nelson, N. B., Siegel, D. A., & Michaels, A. F. (1998). Seasonal dynamics of colored dissolved material in the Sargasso Sea. *Deep-Sea Research Part I*, *45*, 931–957.

O'Reilly, J. E., Maritorena, S., Mitchell, B. G., Siegel, D. A., Carder, K. L., Kahru, M., et al. (1998). Ocean color chlorophyll algorithms for SeaWiFS. *Journal of Geophysical Research*, *103*, 24,937–24,953.

PACE SDT (). A report of the Pre-Aerosol, Clouds, and ocean Ecosystem (PACE) mission science definition team. http://decadal.gsfc.nasa.gov/PACE.html (302 pp., Available at)

Polovina, J. J., Howell, E. A., & Abecassis, M. (2008). Ocean's least productive waters are expanding. *Geophysical Research Letters*, *35*. http://dx.doi.org/10.1029/2007GL031745 (L03618).

Rayner, N. A., Parker, D. E., Horton, E. B., Folland, C. K., Alexander, L. V., Rowell, D. P., et al. (2003). Global analyses of sea surface temperature, sea ice, and night marine air temperature since the late nineteenth century. *Journal of Geophysical Research*, *108*.

Sauer, M. J., Roesler, C. S., Werdell, P. J., & Barnard, A. (2012). Under the hood of satellite empirical chlorophyll a algorithms: Revealing the dependencies of maximum band ratio algorithms on inherent optical properties. *Optics Express*, *20*, 20920–20933.

Siegel, D. A., Behrenfeld, M. J., Maritorena, S., O'Malley, R. T., & Fields, E. (2011). Global ocean phytoplankton [in "State of the Climate in 2010"]. *Bulletin of the American Meteorological Society*, *92*, S105–S108.

Siegel, D. A., Dickey, T. D., Washburn, L., Hamilton, M. K., & Mitchell, B. G. (1989). Optical determination of particulate abundance and production variations in the oligotrophic ocean. *Deep Sea Research*, *36*, 211–222.

Siegel, D. A., Doney, S. C., & Yoder, J. A. (2002a). The spring bloom of phytoplankton in the North Atlantic Ocean and Sverdrup's critical depth hypothesis. *Science*, *296*, 730–733.

Siegel, D. A., & Franz, B. A. (2010). Oceanography: A century of phytoplankton change. *Nature*, *466*, 569–570.

Siegel, D. A., Maritorena, S., Nelson, N. B., & Behrenfeld, M. J. (2005a). Independence and interdependencies of global ocean color properties; Reassessing the bio-optical assumption. *Journal of Geophysical Research*, *110*. http://dx.doi.org/10.1029/2004JC002527 (C07011).

Siegel, D. A., Maritorena, S., Nelson, N. B., Behrenfeld, M. J., & McClain, C. R. (2005b). Colored dissolved organic matter and its influence on the satellite-based characterization of the ocean biosphere. *Geophysical Research Letters*, *32*. http://dx.doi.org/10.1029/2005GL024310 L20605.

Siegel, D. A., Maritorena, S., Nelson, N. B., Hansell, D. A., & Lorenzi-Kayser, M. (2002b). Global distribution and dynamics of colored dissolved and detrital organic materials. *Journal of Geophysical Research*, *107*, 3228. http://dx.doi.org/10.1029/2001JC000965.

Smith, R. C., & Baker, K. S. (1978). The bio-optical state of ocean waters and remote sensing. *Limnology and Oceanography*, *23*, 247–259.

Stramski, D., Boss, E., Bogucki, D., & Voss, K. J. (2004). The role of seawater constituents in light backscattering in the ocean. *Progress in Oceanography*, *61*, 27–56.

Stramski, D., & Kiefer, D. A. (1991). Light scattering by microorganisms in the open ocean. *Progress in Oceanography*, *28*, 343–383.

Sverdrup, H. U. (1955). The place of physical oceanography in oceanographic research. *Journal of Marine Research*, *14*, 287–294.

Swan, C. M., Nelson, N. B., Siegel, D. A., & Kostadinov, T. S. (2012). The effect of surface irradiance on the absorption spectrum of chromophoric dissolved organic matter in the global ocean. *Deep-Sea Research Part I*, *63*, 52–64.

Swan, C. M., Siegel, D. A., Nelson, N. B., Carlson, C. A., & Nasir, E. (2009). Biogeochemical and hydrographic controls on chromophoric dissolved organic matter distribution in the Pacific Ocean. *Deep-Sea Research Part I*, *56*, 2172–2192.

Szeto, M., Werdell, P. J., Moore, T. S., & Campbell, J. W. (2011). Are the world's oceans optically different? *Journal of Geophysical Research*, *116*. http://dx.doi.org/10.1029/2011JC007230.

Toole, D. A., Siegel, D. A., & Doney, S. C. (2008). A light-driven, one-dimensional dimethylsulfide biogeochemical cycling model for the Sargasso Sea. *Journal of Geophysical Research*, *113*. http://dx.doi.org/10.1029/2007JG000426 (G02009).

Torrecilla, E., Stramski, D., Reynolds, R. A., Millán-Núñez, E., & Piera, J. (2011). Cluster analysis of hyperspectral optical data for discriminating phytoplankton pigment assemblages in the open ocean. *Remote Sensing of Environment*, *115*, 2578–2593.

Vantrepotte, V., & Mélin, F. (2009). Temporal variability of 10-year global SeaWiFS time-series of phytoplankton chlorophyll a concentration. *ICES Journal of Marine Science: Journal du Conseil*. http://dx.doi.org/10.1093/icesjms/fsp107.

Vantrepotte, V., & Mélin, F. (2011). Inter-annual variations in the SeaWiFS global chlorophyll a concentration (1997–2007). *Deep-Sea Research Part I*, *58*, 429–441.

Werdell, P. J., & Bailey, S. W. (2005). An improved bio-optical data set for ocean color algorithm development and satellite data product validation. *Remote Sensing of Environment*, *98*, 122–140.

Westberry, T. K., Behrenfeld, M. J., Siegel, D. A., & Boss, E. (2008). Carbon-based primary productivity modeling with vertically resolved photoacclimation. *Global Biogeochemical Cycles*, *22*. http://dx.doi.org/10.1029/2007GB003078 (GB2024).

Westberry, T. K., Dall'Olmo, G., Boss, E., Behrenfeld, M. J., & Moutin, T. (2010). Coherence of particulate beam attenuation and backscattering coefficients in diverse open ocean environments. *Optics Express*, *18*, 15419–15425.

Xue, Y., Reynolds, R. W., Banzon, V., Smith, T. M., & Rayner, N. A. (2011). Sea surface temperatures in 2010. In "State of Climate 2010". *Bulletin of the American Meteorological Society*, *92*, S78–S81.

Yamashita, Y., & Tanoue, E. (2009). Basin scale distribution of chromophoric dissolved organic matter in the Pacific Ocean. *Limnology and Oceanography*, *54*, 598–609.

Yoder, J. A., & Kennelly, M. A. (2003). Seasonal and ENSO variability in global ocean phytoplankton chlorophyll derived from 4 years of SeaWiFS measurements. *Global Biogeochemical Cycles*, *17*. http://dx.doi.org/10.1029/2002GB001942.

Yoder, J., McClain, C. R., Feldman, G. C., & Esaias, W. E. (1993). Annual cycles of phytoplankton chlorophyll concentrations in the global ocean: A satellite view. *Global Biogeochemical Cycles*, *7*, 181–193.

Zepp, R. G., Erickson, D. J., III, Paul, N. D., & Sulzberger, B. (2007). Interactive effects of solar UV radiation and climate change on biogeochemical cycling. *Photochemical & Photobiological Sciences*, *6*, 286–300.